Environmental and Experimental Botany 228 (2024) 105982

Contents lists available at ScienceDirect

Environmental and Experimental Botany

journal homepage: www.elsevier.com/locate/envexpbot

Research paper

# At the core of salinity: Divergent transcriptomic responses to neutral and alkaline salinity in *Arabidopsis thaliana*

Maria Almira-Casellas [a,1], Sílvia Busoms [a,*,2], Laura Pérez-Martín [a,3], Glòria Escolà [a,4], Álvaro López-Valiñas [b,5], Antoni Garcia-Molina [c,6], Mercè Llugany [a,*,7], Charlotte Poschenrieder [a,8]

[a] Plant Physiology Unit, Biosciences Faculty, Universitat Autònoma de Barcelona (UAB), Bellaterra 08193, Spain
[b] Unitat Mixta d'Investigació IRTA-UAB en Sanitat Animal, Centre de Recerca en Sanitat Animal (CReSA), Campus UAB, Bellaterra 08193, Spain
[c] Centre for Research in Agricultural Genomics (CRAG), NSIC-IRTA-UAB-UB, Barcelona, Spain

ARTICLE INFO

*Keywords:*
*Arabidopsis* demes
Abiotic stress
Alkaline salinity
Transcriptome
WGCNA

ABSTRACT

In the context of current climate change, alkaline salinity is increasingly challenging crop yields, especially in arid and semiarid regions. Alkaline salinity is more detrimental to plant performance than neutral salinity and tolerance to neutral salinity may not confer tolerance to alkaline salinity. The mechanisms behind are still poorly understood. This study aims to identify physiological and genetic traits underlying this differential tolerance to neutral and alkaline salinity by exploiting the variation present in natural populations (demes) of *Arabidopsis thaliana*. Growth, photosynthesis, phytohormone and mineral nutrient profiles, plant water status and transcriptomic changes were analyzed in four demes with contrasting tolerance to neutral and alkaline salinity. Results of this novel holistic approach suggest low internal Fe use efficiency caused by bicarbonate as a driver of enhanced sensitivity to alkaline salinity in plants adapted to neutral salinity prompting photosynthesis inhibition and alteration of the plant's carbon budget for primary and secondary metabolism. Moreover, alkaline salinity specifically altered the auxin and jasmonic acid signaling pathways, while sustained ABA biosynthesis was an adaptive trait under neutral salinity. Exploring the genes with non-shared expression trends between salinity types, we identified sequence variation at the *BGAL4* locus associated with advantageous responses to each type of salinity. Weighted correlation network analysis (WGCNA) validated the significant involvement of gene co-expression modules targeted by the enrichment analyses, highlighting the hubs correlated with favorable responses to both salinity types. Overall, the present study points out the complex physiological and genetic mechanisms responsible for plant tolerance to alkaline salinity and proposes target genes for breeding strategies under alkaline saline soils.

## 1. Introduction

Saline stress is a major agricultural constraint and its co-occurrence with alkalinity is an arising environmental concern, especially under arid and semiarid climates. Based on the FAO/UNESCO soil map of the world, more than one million hectares of the Earth's land are affected by

* Corresponding authors.
*E-mail addresses:* mariajose.almira@uab.cat (M. Almira-Casellas), silvia.busoms@uab.cat (S. Busoms), laura.perezmartin@unige.ch (L. Pérez-Martín), gloria.escola@uab.cat (G. Escolà), alvaro.lopezv@irta.cat (Á. López-Valiñas), antoni.garcia@cragenomica.es (A. Garcia-Molina), merce.llugany@uab.cat (M. Llugany), charlotte.poschenrieder@uab.es (C. Poschenrieder).
[1] 0000-0002-4035-8766
[2] 0000-0002-9917-7118
[3] 0000-0001-6066-3939
[4] 0000-0003-4231-4334
[5] 0000-0002-7492-5108
[6] 0000-0002-7790-9736
[7] 0000-0002-9940-0383
[8] 0000-0002-3818-0874

https://doi.org/10.1016/j.envexpbot.2024.105982
Received 7 March 2024; Received in revised form 23 August 2024; Accepted 19 September 2024
Available online 9 October 2024

alkaline salinity stress. This is the case of the Mediterranean region, where excess of soluble $Na^+$, $Ca^{2+}$, $Mg^{2+}$, $K^+$, $CO_3^{2-}$ and $HCO_3^-$ ions get to the superficial soil layers due to high evapotranspiration rates (Singh, 2021). In addition to the common stress factors shared with neutral salinity, i.e. osmotic, ion and ROS stresses, alkaline salinity exacerbates nutrient deficiency (Liu et al., 2021) and exerts stronger inhibition on germination, growth, photosynthesis, and root system activity (Guo et al., 2010; 2017; Marconi et al., 2013).

There is increasing evidence that alkaline salinity is more detrimental for overall plant performance than neutral salinity, but the mechanisms driving such exacerbated effects are not yet clearly established. In this regard, exploiting natural genetic and phenotypic variation caused by the environmental factors that generate local-scale diversity patterns is essential (Bomblies et al., 2010). In the model plant *Arabidopsis thaliana*, differences in tolerance to salinity and moderate levels of carbonate as individual stress factors have been described among natural populations (demes) in the NE region of Catalonia, Spain (Busoms et al., 2015; Terés et al., 2019). Such comparative analyses also revealed that tolerance to neutral salinity does not confer tolerance to alkaline salinity in *A. thaliana* (Pérez-Martín et al., 2022). In fact, demes from neutral saline soils exhibited the highest sensitivity to alkaline salinity, whereas demes from soils with moderate salinity and carbonate levels outperformed the rest of individuals under alkaline salinity stress (Pérez-Martín et al., 2022). However, the transcriptomic basis of such differential responses was not explored.

The effects of co-occurrence of salinization and alkalization has mainly been described in crop species like cotton (Zhang et al., 2018), wheat (Sun et al., 2020), rapeseed (Meng et al., 2017), alfalfa (An et al., 2016), soybean (Jin et al., 2022) and rice (Li et al., 2018). Such studies report nutrient and redox homeostasis, and changes in endogenous phytohormone levels among the most important mechanisms conferring tolerance to neutral and alkaline salinity. Information in *A. thaliana* is scarce. However, the occurrence of natural populations differing in tolerance to alkaline salinity provides a unique tool for exploring the naturally evolved mechanisms underlying alkaline salinity tolerance in a model glycophyte species. Here, we combine physiological studies with transcriptomic analyses to provide a deeper understanding of the related biological processes (Yang et al., 2022). Linking changes in gene expression profiles to functional consequences is the ultimate goal of transcriptomic analysis on stress tolerance-related traits (Yan et al., 2020). The specific aim of the present study is to identify the levels and functions of plant stress regulatory networks underlying two contrasted types of soil salinity: neutral and alkaline. To this end, we searched for shared and exclusive responses of *A. thaliana* to both stress conditions among 2 demes locally adapted to neutral saline (NS) and 2 demes from moderate alkaline saline (AS) soils. The studied demes were referred to as NS1, NS2, AS1 and AS2. The physiological and transcriptomic responses of the 4 demes under each type of salinity were analyzed, and the convergent and singular metabolic pathways involved in each type of salinity are described. Finally, co-expression network analysis correlating transcriptomics with physiological data was performed to identify hub pathways in shared and unique plant responses to neutral and alkaline salinity.

## 2. Material & Methods

### 2.1. Plant material

Seeds of plants from 2 coastal-siliceous (NS1 and NS2) and 2 prelittoral calcareous sites (AS1, AS2) *A. thaliana* demes were collected (Figure A2) and propagated in the laboratory. The flowchart in Figure A3 summarizes the experimental procedures of the study.

### 2.2. Irrigation experiment

Seeds were surface sterilized by soaking them in 30 % (v/v) commercial Clorox bleach and 1 drop of Tween-20 for 15 min and rinsed 5 times in 18 MΩmilli-Q sterile water. Seeds were stratified at 4ºC for 1 week in the dark and sowed on wet soil. Pots were covered with PVC film until the seedlings germinated. Pots with germinated seedlings were placed in a growth chamber (Conviron CMP5090) with 8 h light / 16 h dark photoperiod, an irradiance of 80 $mmol \cdot m^{-2} \cdot s^{-1}$ and a constant temperature of 22 ºC. Plants were watered with 0,5-strength Hoagland solution every 3 days. After 2 weeks, all plants were irrigated every 3 days with 0,5-strength Hoagland solution containing 0,5-strength Hoagland solution alone at pH 6 (control), with 100 mM NaCl at pH 6 (neutral salinity: ***neuSAL***) or with 85 mM NaCl and 15 mM $NaHCO_3$ at pH 8.3 (alkaline salinity, ***alkSAL***) for two weeks. The Rosette Diameter (RD) and the PSII efficiency of each sample were measured after two weeks of treatment. After harvest, samples for ionomic analysis were dried and samples for RNA extraction and hormone determination were immediately frozen in liquid nitrogen and stored at −80 ºC.

### 2.3. Mineral nutrient analysis

Plant tissues were sampled by removing 2–3 leaves or cutting roots (1–5 mg dry weight). They were then washed with 18 MΩ water before placing them in Pyrex digestion tubes. The sampled plant material was dried for 2 days at 60 ºC and weighed before open-air digestion in Pyrex tubes using 0.7 mL concentrated $HNO_3$ at 110 ºC for 5 h in a hot-block digestion system (SC154–54-Well Hot Block, Environmental Express, Charleston, SC, United States). Concentrations of the selected elements (Ca, K, Mg, Na, P, S, Mo, Cu, Fe, Mn, Zn) were determined by ICP-MS (Perkin ElmerInc., ELAN 6000, MA, United States) or ICP-OES (Thermo Jarrell-Ash, model 61E Polyscan, England) (n=6 per deme and treatment).

### 2.4. PSII efficiency

The maximal photochemical efficiency of PSII was calculated from the ratio of variable (Fv) to maximum (Fm) fluorescence [$F_v/F_m = (Fm - F_o)/F_m$] using a MINI-PAM-II/B portable chlorophyll fluorometer (Walz) connected to an Arabidopsis Leaf Clip holder (model 2060-B). The minimum fluorescence yield ($F_o$) was measured under measuring light (650 nm) with very low intensity (0.8 mmol $m^{-2}$ $s^{-1}$). To estimate the maximum fluorescence yield ($F_m$), a saturating pulse of white light (3000 mmol $m^{-2}$ $s^{-1}$ for 1 s) was applied. Leaves were dark-adapted for 30 min before measurements and the analysis was performed in a dark room with stable ambient conditions (n=6 per deme and treatment).

### 2.5. Endogenous phytohormones

Phytohormones extraction was done according to the protocol of Pan et al. (2008) with modifications from Delatorre et al. (2017). The phytohormones analyzed were (+)-cis, trans-abscisic acid (ABA), 3-indoleacetic acid (IAA), 1-aminocyclopropane-1-carboxylic acid (ACC), (±)-jasmonic acid (JA), and salicylic acid (SA). The following deuterated standards were employed: ABA-$^2$H6, IAA-d5, ACC-d4, JA-d5, and SA-d6. All of them were supplied by Olchemim Ltd. (Czech Republic) except SA-d6 obtained from Sigma Aldrich (St. Louis, MO, USA). Briefly, 0.05 g fresh weight of leaf samples were homogenized in liquid $N_2$ and extracted with 250 μL of extraction buffer (2- propanol/Mili Q water/-Hydrochloric acid; 2:1:0.002; v/v/v) in 1.5 mL Eppendorf tubes (Eppendorf Safe Lock England) and agitated by repeated inversion (60 rpm) for 20 min, at 4 ºC, in the dark. The resulting homogenate was transferred to a Teflon tube (Thermo Scientific, England) with 450 μL dichloromethane and reextracted by repeated and inverted agitation for 30 min, at 4 ºC in the dark. Three phases were obtained, an aqueous, a material debris and an organic phase. The organic phase (bottom) was recovered, and the intermediate debris phase was also re-extracted. The combined extracts were evaporated under $N_2$ flow to remove propanol and resuspended 150 μL of 100 % methanol. Resuspended extracts were

filtered through a 0.22 μm cellulose acetate Spin-X centrifuge tube filter (Costar, Corning Inc., Salt Lake City, USA). Samples were injected into a QTrap4000 LC–ESI(−)–MS/MS system following the method described by Segarra et al. (2006) and modified by Llugany et al. (2013) using HPLC Agilent 1100 (Waldrom, Germany) on a Discovery C18 2.1 × 150 mm ID, 5 μm column (Supelco, Bellefonte, USA) at 50 ºC, a constant flow rate of 0.6 mL min−1 and 10 μL injected volume. MS/MS experiments were performed on an API 3000 triple quadrupole mass spectrometer (PE Sciex, Concord, Ontario, Canada). All the analyses were performed using the Turbo Ionspray source in negative ion mode for SA, JA, ABA, IAA, and PAA and in positive mode for ACC. Quantification was performed by injection of extracted and spiked samples in multiple reaction monitoring (MRM) mode (n=6 per deme and treatment).

### 2.6. Transcriptome profiling

#### 2.6.1. Total RNA Exaction and RNA-Seq Library Preparation

Total RNA was extracted using Maxwell plant RNA kit (Promega Corporation, Madison, WI, USA) following the manufacturer's instruction. The RNA concentration was measured using Qubit® 2.0 Fluorometer (Invitrogen). 4 μg total RNA was used to prepare RNA-seq libraries using the TruSeq Stranded mRNA Library Prep Kit (Illumina, San Diego, US). Strand specific paired-end mRNA sequencing was performed on DNBSEQ platform at the Next-Generation Sequencing Core of the BGI GenomiNS Service (Hong Kong, China) (n=3 per deme and treatment). The RNA Integrity Number (RIN) was assessed by the Agilent 2100 Bioanalyzer System (Agilent Technologies, Inc., Santa Clara, California, USA). Following sample requirements for plant RNA processing, samples with RNA concentration greater than 20 ng/uL and RIN value above 6 were selected for analysis. One sample was excluded for not meeting the general requirements (Dataset B16).

#### 2.6.2. RNA-Seq analysis

Bowtie2 (Langmead and Salzberg, 2012) was used to map the clean reads to the *Arabidopsis thaliana* genome (Araport11), and then RSEM (Li and Dewey, 2011) was used to calculate the transcript abundance of each sample. Quality check of raw sequence data was performed using Fastqc. Reads containing adapters and poly-N and low-quality reads from raw data were removed with Qualimap. Simultaneously, Q20 (percentage of bases with the quality score greater than 20; sequencing error rate less than 1 %), Q30 (percentage of bases with the quality score greater than 30; sequencing error rate less than 0.1 %), and GC (or guanine-cytosine) content of the clean data were calculated. Paired-end reads were mapped to the TAIR10 reference genome using the STAR aligner and the.sam output of STAR was then converted to its compressed format.bam and sorted by gene identifier with samtools. The overlap of reads with annotation features found in the reference.gtf was calculated using HT-seq (Putri et al., 2022).

The output computed for each sample (raw read counts) was imported into BGI data visualization system (https://www.bgi.com/global/service/dr-tom) and parsed using DESeq2 (v 1.8.1). Raw counts were normalized using DESeq2's function "rlog," which normalizes sequences according to library size to make them comparable among replicates and transforms the original count data to the log scale. The DEseq2 method is based on the principle of negative binomial distribution (Love et al., 2014). This method was used to perform differential gene expression analysis (DEG) with an absolute |FC= > 2. The *p*-values were corrected for multiple error testing according to Benjamini-Hochberg (*q*-value) and *q*-value threshold of 0.05 was set. According to the results of differential gene detection, the R package *pheatmap* was used to perform hierarchical clustering analysis and extract expression trends on the union set differential genes.

#### 2.6.3. Quantitative real-time PCR validation

Six genes representing a wide range of expression profiles were selected for verification of RNA-seq data using quantitative real-time PCR (qRT-PCR) (Figure A1, Dataset B17). Total RNA of about 100 mg of plant leaf material was extracted using the MaxwellR RSC plant RNA kit (Promega Corporation, WI, United States). Two micrograms of total RNA were used as a template to synthesize first-strand cDNA with the iScriptTM cDNA Synthesis Kit (Bio-Rad, United States). The cDNA was used as a template for Reverse-Transcriptase quantitative real-time PCR (RT-qPCR) using iTaqTM Universal SYBR Green Supermix (Bio-Rad, CA, United States). Real-time detection of fluorescence emission was performed on a CFX384 Real-Time System (Bio-Rad, CA, United States), and plates were edited using the CFX manager version 3.1 software. Relative quantifications were performed for all genes with the Actin2 gene (AT3G18780) used as an internal reference. For each sample, the average value from triplicate RT-qPCRs was used to estimate transcript abundance. The mean Ct values were normalized against Actin2 and dCt values were calculated as (dCtGene- dCtActin2). The data are expressed as means ± SE.

#### 2.6.4. Gene functional annotation

Gene Onthology (GO) functional significant enrichment analysis - used to analyze molecular functions, cellular components and biological processes - was performed by mapping all candidate genes to each entry in the Gene Ontology database (http://www.geneontology.org/). A hypergeometric test was applied to find the GO function significantly enriched in candidate genes compared to all background genes of the species. *p*-value was calculated using the basis function phyper (https://stat.ethz.ch/R-manual/R-devel/library/stats/html/Hypergeometric.html) of R and then corrected for multiple error testing according to Benjamini-Hochberg

(https://bioconductor.org/packages/release/bioc/html/qvalue.html). Finally, a *q*-value threshold of 0.05 was set, and the GO term that satisfied this condition was defined as the GO term that was significantly enriched in candidate genes. Kyoto Encyclopedia of Genes and Genomes (KEGG) pathway-based enrichment analysis – which links gene sets with a network of interacting molecules in the cell, such a pathway or complex - was performed following the same methodology and significance threshold than for GO functional enrichment analysis. Pathways significantly enriched in differentially expressed genes were identified and visualized through BGI data visualization system (https://www.bgi.com/global/service/dr-tom)

#### 2.6.5. Protein-Protein Interaction (PPI) Network Analysis

Protein–protein Interaction (PPI) networks of differential expressed genes were performed on STRING version 11.0. Active interaction sources, including text mining, experiments, databases, and co-expression as well as species limited to "*Arabidopsis thaliana*" and an interaction score > 0.4 were applied to construct the PPI networks.

#### 2.6.6. WGCNA network analysis

Weighted gene co-expression network analysis (WGCNA) was conducted with the "WGCNA" package (Langfelder and Horvath, 2008) on BGI's Dr.Tom system (http://biosys.bgi.com). Gene expression file and trait file were combined, and the soft thresholding power (β value) was filtered based on the calculation of scale-free topological fit index and mean connectivity. The topological overlap matrix (TOM) was constructed based on the topological overlap between pairwise genes, and hierarchical clustering analysis was performed. Cluster dendrogram plot and clustering tree of co-expression modules of DEGs were created. The co-expression relationships among different modules were analyzed and modules with high similarity were merged at a similarity threshold of 0.25 and a minimum module size of 20 genes.

### 2.7. Statistical Analysis

All statistical analyses were performed using JMP SAS software (SAS Institute, Cary, NC, United States). Significant differences for multiple comparisons were determined by one-way or two-way ANOVA as

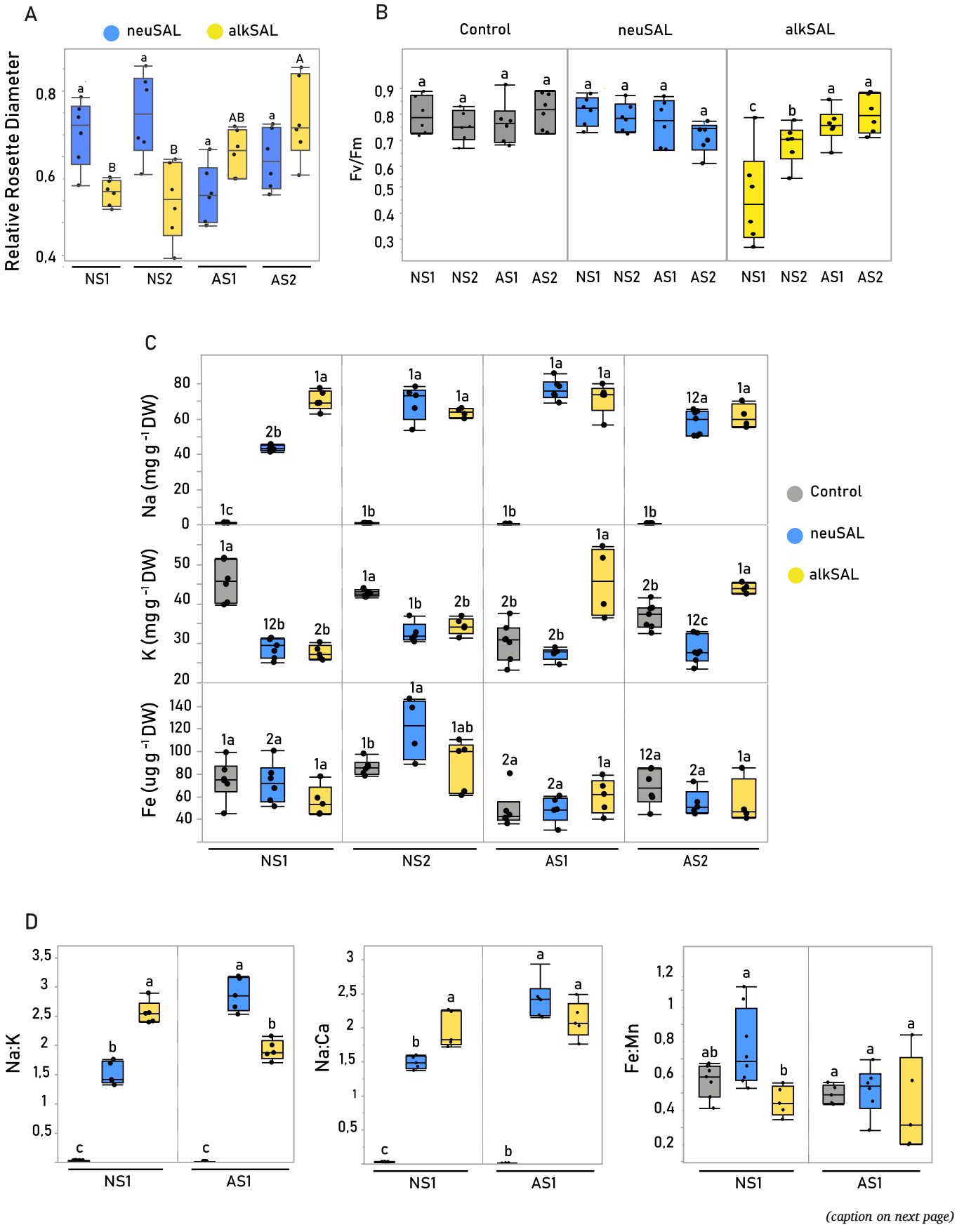


*(caption on next page)*

**Fig. 1. Leaf growth, photosynthesis efficiency and mineral nutrition in *A. thaliana* demes under control (C), neutral (*neuSAL*) and alkaline (*alkSAL*) salinity. (A)** Mean ± SE of growth (relative rosette diameter) of each deme and treatment. Each dot represents a biological replicate (n=6). Mean values with different letters indicate significant differences (Tukey's HSD, adj. *p*-value < 0.05). (B) Mean ± SE of Maximum PSII photochemical efficiency ($F_v/F_m$) of each deme and treatment. Each dot represents the mean value of 2 technical replicates (2 measurements on each biological replicate) (n=6). Mean values with different letters indicate significant differences (Tukey's HSD, adj. *p*-value < 0.05). (C) Na (mg $g^{-1}$ DW), K (mg $g^{-1}$ DW) and Fe concentration (ug $g^{-1}$ DW) in plant leaf samples from each deme and treatment. Each dot represents a biological replicate (n=6). Letters indicate significant differences among treatments per each deme (Tukey's HSD, adj. *p*-value < 0.05); numbers indicate significant differences among demes on each treatment (Tukey's HSD, adj. *p*-value < 0.05) (D) Mean ± SE of analyzed nutrient ratios in the carbonate sensitive deme NS1 and the carbonate tolerant AS1. Each dot represents a biological replicate (n=6). Mean values with different letters indicate significant differences between treatments (Student *t*-Test, adj. *p*-value < 0.05). Plants were grown in potting mix soil and irrigated with C (0.5-Hoagland, pH 5.9), *neuSAL* (100 mM NaCl, pH 5.9) or *alkSAL* (85 mM NaCl, 15 mM $NaHCO_3$, pH 8.3) for 2 weeks.

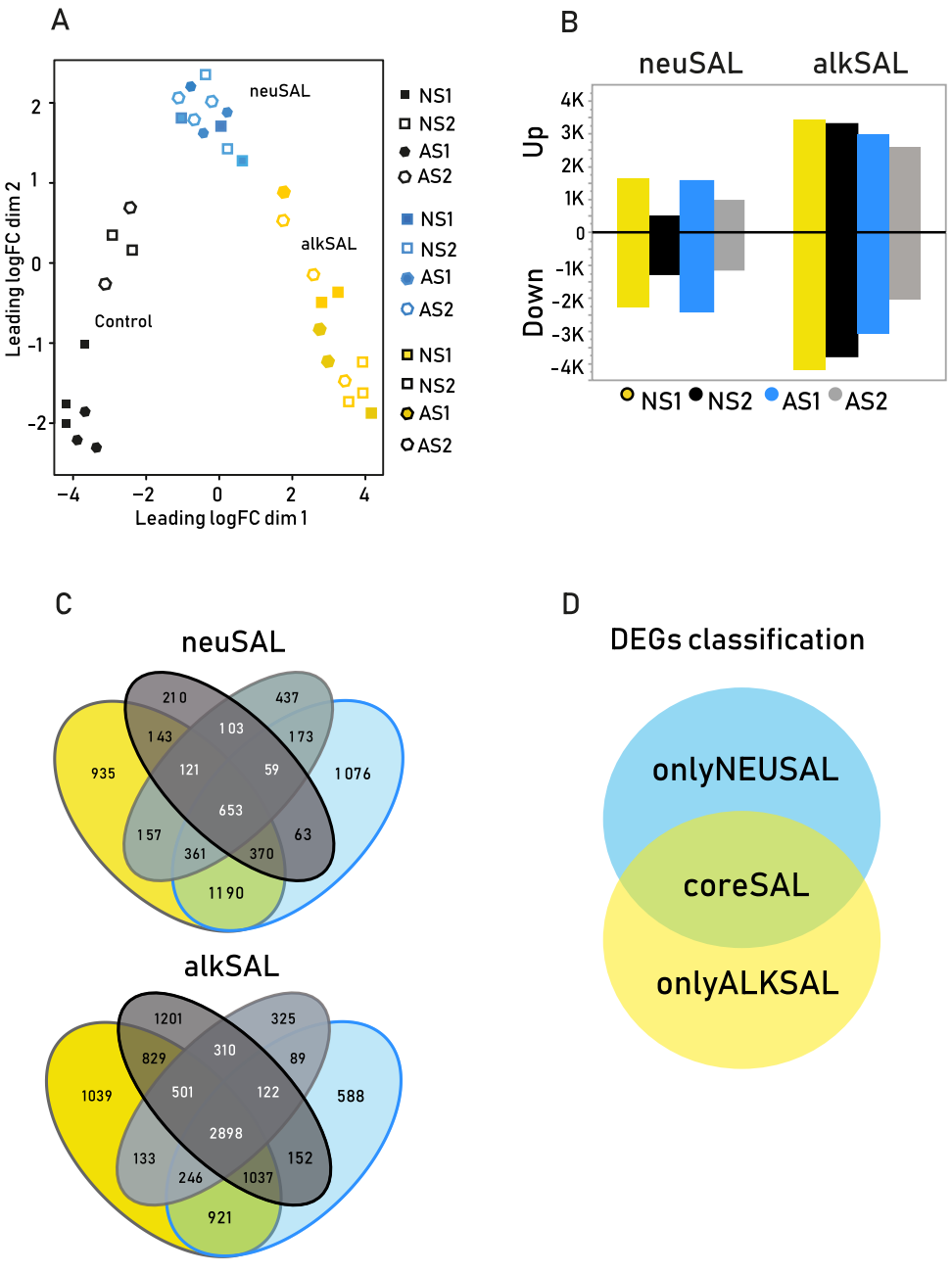


**Fig. 2. Differential Gene Expression (DEG) analysis in *A. thaliana* demes NS1, NS2, AS1, and AS2. (A)** Multidimensional scaling (MDS) plot of RNA expression profiles in the studied samples. Sample relations are plotted using a multidimensional scaling plot (MDS) generated with edgeR showing the variability between replicates and treatments in log2-fold-change distance. The axes represent gene expression levels between the different experimental factors. Each dot represented a sample, color coded by treatment (Black: Control, Blue: *neuSAL*, Yellow: *AlkSAL*) and shape coded by deme (Color-filled square: NS1, empty square: NS2, color-filled octagon: AS1, empty octagon: AS2). **(B)** Histogram showing the number of differentially expressed genes for each deme (n=3) and treatment (*neuSAL*/Control; *alkSAL*/Control). **(C)** Venn diagram showing the mutual overlaps of DEGs among demes under each treatment. DEGs were filtered at log fold change (LFC > 2, LFC < −2), and *q*-value (FDR-adjusted *p*-value) < 0.05.

indicated in figure legends, treatment or treatment relative to control (neuSAL/Control; alkSAL/Control) and deme (NS1, NS2, AS1, AS2) or deme origin [$NS_{(NS1+NS2)}$; $AS_{(AS1+AS2)}$] as independent factors. Comparisons among demes were followed by post hoc Tukey HSD test (adjusted $p$-value $< 0.05$). Multivariate Correlation Analysis (MCA) was performed to determine the level of association among the measured physiological traits for each deme and treatment. Pearson's correlation coefficients were calculated for all pairs of measured parameters under *neuSAL* and *alkSAL* at a level of 5 % significance. Principal Component Analysis, eigenvalues and relative proportion of the variance explained by each trait included in MCA were calculated.

## 3. Results & Discussion

### 3.1. Demes from coastal siliceous soils display reduced growth and photosynthesis under alkaline salinity

The four *Arabidopsis thaliana* demes (NS1, NS2, AS1, AS2) were subjected to 0 mM NaCl at pH 6 (***control***), 100 mM NaCl at pH 6 (neutral salinity: ***neuSAL***) or with 85 mM NaCl and 15 mM $NaHCO_3$ at pH 8.3 (alkaline salinity, ***alkSAL***) for two weeks. Overall, *neuSAL* and *alkSAL* caused 50 % decrease in relative rosette diameter (RD) [$(RD_{Treatment})/(RD_{Control})$] regardless of deme and treatment. However, NS demes (NS1 and NS2) showed a significant reduction in rosette diameter size under *alkSAL* when compared to *neuSAL*. On the opposite, AS demes (AS1, AS2) exhibited higher relative rosette diameter under *alkSAL* than under *neuSAL* and significantly better growth maintenance than NS demes under *alkSAL* conditions ($p$-value $\leq 0.05$, Tukey's HSD) (Fig. 1A; Dataset B1).

No significant differences in Fv/Fm among demes were observed under control and *neuSAL* conditions, where the mean values of Fv/Fm were within the optimum for stress-free plants (between 0.79 and 0.84) (Maxwell and Johnson 2000). On the contrary, under *alkSAL*, AS1 (mean $F_v/F_m = 0.770$) and AS2 (mean $F_v/F_m = 0.820$) maintained better $F_v/F_m$ than NS1 and NS2 ($p$-value $\leq 0.05$, Tukey's HSD). Remarkably, NS1 displayed a dramatic decrease in $F_v/F_m$ values (mean $F_v/F_m = 0.520$) when compared to the rest (Fig. 1B; Dataset B2). The chlorophyll (Chl) fluorescence parameter, Fv/Fm, reflects the maximum quantum efficiency of PSII photochemistry in the dark-adapted state and has been widely used for the detection of early stress responses in plants (e.g. Kalaji et al., 2018). Reduction of total photosynthetic activity is a common feature of plant stress, and these results confirm that the ability to maintain the photosynthetic capacity is a good indicator of tolerance to either *neuSAL* or *alkSAL* in *A. thaliana*.

The above observations point to a better performance of demes from pre-littoral calcareous soils (AS1, AS2) under *alkSAL* in terms of growth maintenance and photosynthesis, which agrees with the severe reduction in plant growth previously reported on carbonate sensitive demes under *alkSAL* conditions (Pérez-Martín et al., 2022).

### 3.2. Alkaline salinity disrupts leaf nutrient distribution in demes adapted to neutral salinity

Is it well known that both neutral and alkaline salinity disrupts nutrient availability, transport and partition, reducing plant growth and photosynthesis efficiency (Hu & Schmidhalter, 2005; Baxter et al., 2012; Almira-Casellas et al., 2023). To explore whether neutral and alkaline salinity differentially affect mineral nutrition, elemental profiling of leaf tissue was performed in all samples (Dataset B3). Although nutrient profiles of each deme were genotype-specific (Figure A2), divergent responses dependent on deme origin were observed for $Na^+$ and $K^+$ (Fig. 1C). Under *neuSAL* NS1 accumulated significantly less leaf $Na^+$ than any other deme, whereas the highest leaf $Na^+$ accumulation was reported in AS1. Moreover, the increased leaf $Na^+$ detected in NS2 was attributed to its reported allelic variation at the HKT1;1 locus, which leads to higher shoot $Na^+$ accumulation and enhanced $Na^+$ tolerance (Rus et al., 2006; Busoms et al., 2018) (Fig. 1C). Under *alkSAL*, AS demes shared enhanced $K^+$ retention when compared to NS demes (Fig. 1C), a strategy which confers salinity tolerance (Wang et al., 2007; Shabala and Cuin, 2008).

Under *neuSAL*, NS1 maintained a significantly lower Na:K, and higher Na:Ca than under *alkSAL*. The cellular $Na^+$ and Ca transport pathways are linked via SOS2 (a ser/thr protein kinase activated by SOS3, a calcium sensor protein). *SOS2* regulates *SOS1* and *NHX1* (plasma membrane and tonoplast $Na^+/H^+$ antiporters), but also *CAX1* (a vacuolar $Ca/H^+$ antiporter) (Cheng et al., 2004). Decreasing the Na:Ca ratio can improve $K^+$ uptake and reduce $Na^+$ uptake, ultimately decreasing Na:K (Garg et al., 2015).

Although alkaline conditions hamper iron acquisition (Liu et al., 2024), no significant differences in Fe concentrations were found among demes under neutral and alkaline salinity (Fig. 1C). It is well established that bicarbonate sensitive plants with Fe-deficiency symptoms may have relatively high total leaf iron concentrations (Römheld, 2000). This so-called "iron paradox" (Römheld, 1987), is a consequence of bicarbonate-induced alteration of Fe distribution causing tissue accumulation of biologically inactive iron (FeIII) (Lucena, 2000). Either or both bicarbonate-induced alterations in the carbon metabolism (Lopez-Millan et al., 2013; Busoms et al., 2023) and interference with manganese (Rai et al., 2021) may contribute to this phenomenon. In fact, under *alkSAL* NS1 exhibited a significantly lower leaf Fe:Mn ratio than under neutral salinity. Fe and Mn share transporters (e.g. IRT1), and Fe-deficiency symptoms in *A. thaliana* can be alleviated by sequestration of Mn in root vacuoles to maintain Fe:Mn balance (Eroglu et al., 2016).

The differential responses of the nutrient profiles to neutral and alkaline salinity of our contrasting demes indicate that in NS there is a geographical footprint of adaptation to neutral but not to alkaline salinity, which reinforces the statement that tolerance to salinity in siliceous soils does not confer tolerance to alkaline salinity (Pérez-Martín et al., 2022).

### 3.3. Transcriptome profiling confirms exacerbated effects of alkaline salinity on NS demes

Leaf transcriptome profiling of the 4 demes cultivated under control, *neuSAL* or *alkSAL* conditions was performed to characterize the mechanisms underlying the differential response to neutral and alkaline salinity at the gene expression level. Multi-Dimensional Scaling (MDS) was used to visualize global transcriptional similarity among samples (Fig. 2A). The transcriptome of each sample was shaped by deme and colored by treatment. Accordingly, individuals showed major transcriptional similarity between samples corresponding to the same treatment, indicating that the transcriptomic response was treatment specific. Differentially expressed genes (DEGs) per deme and treatment were expressed based on absolute $\log_2$ fold-change (FC) $> 2$ under each treatment compared to control conditions (*neuSAL*/Control, *alkSAL*/Control) ($q$-value $< 0.05$, Wald test). A total of 6164 DEGs (2559 up-regulated and 3605 down-regulated) were identified under *neuSAL* and 10487 DEGs (4995 up-regulated and 5492 down-regulated) under *alkSAL* (Fig. 2B). Under *alkSAL*, NS1, NS2, AS1 and AS2 displayed 1.9, 4.1, 2.2 and 1.53-times more DEGs than under *neuSAL*. Under *alkSAL*, NS1 showed the most altered transcriptome, followed by NS2 (73 % and 68 % of total *alkSAL* DEGs, respectively), while AS1 and AS2 transcriptomic response was more attenuated (58 % and 44 % of total DEGs) (Fig. 2B-C). These results provide evidence that alkaline salinity involves more complex processes than neutral salinity at the transcriptomic level (Fang et al., 2021) and that carbonate-sensitive demes show greater transcriptome alteration after prolonged exposure to *alkSAL*.

It is well known that plants facing complex stress conditions trigger a cascade of signals unique to specific stress components as well as shared responses (Zandalinas et al., 2021; Skalak et al., 2021). To get an overview of the unique and shared molecular components of neutral and

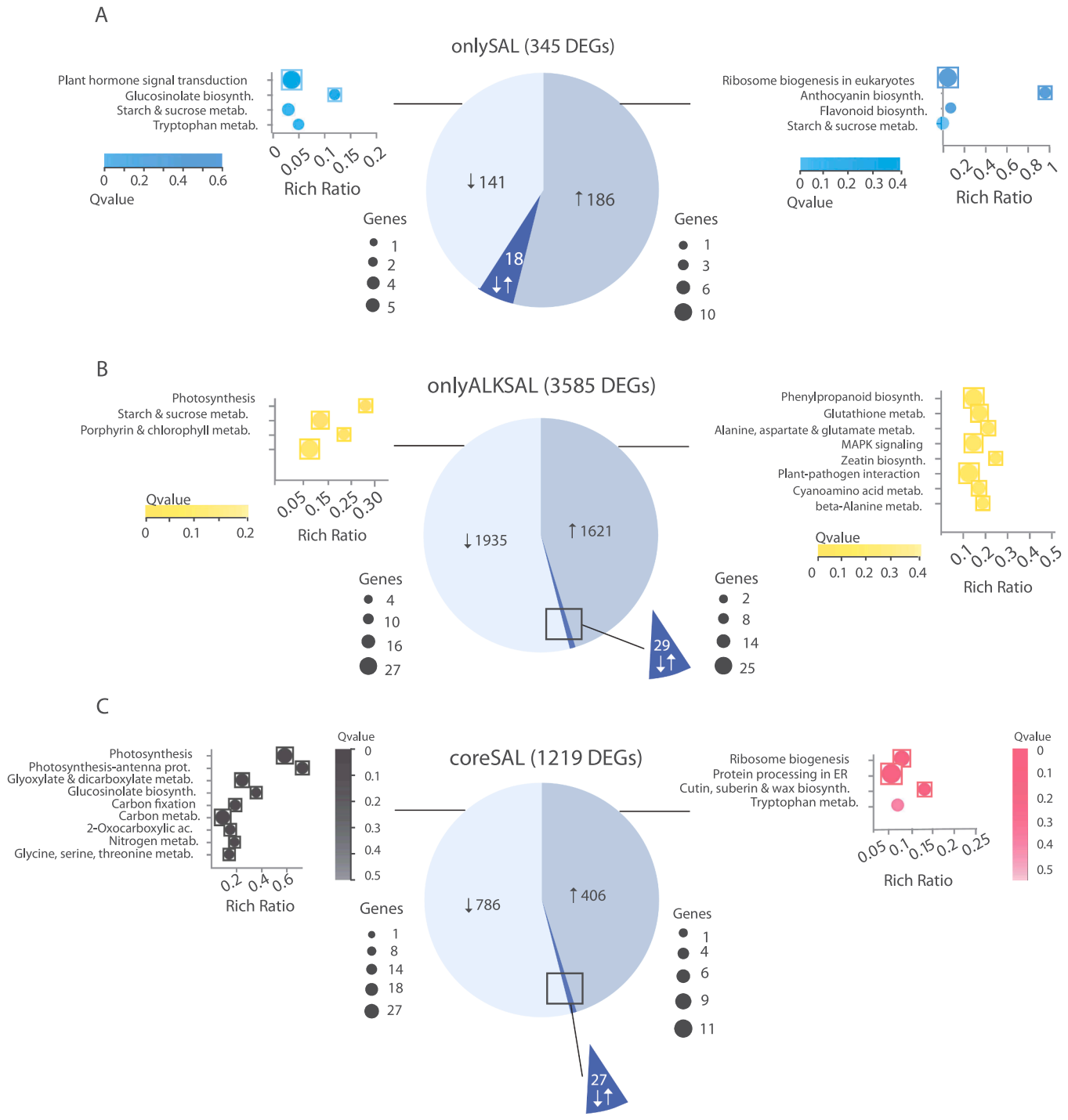


**Fig. 3. Characterization of the onlySAL, onlyALKSAL and coreSALs sets.** DEGs were filtered at log fold change (LFC > 2, LFC < −2), and q-value (FDR-adjusted p-value) < 0.05. Chart pies show expression trends of total **(A)** *onlySAL*, **(B)** *onlyALKSAL* and **(C)** *coreSAL* DEGs. KEGG pathway enrichment analyses of down-regulated (bubble plot, left) and upregulated DEGs (bubble plot, right) are shown for each corresponding DEG set. In bubble plots, pathways belonging to different classifications are listed on the left. Only significant pathways are shown, which are sorted by the q-value. Rich ratio (x-axis) is the ratio of the DEG number to the total gene number in a certain pathway. Bubble size represents the number of DEGs included in each pathway (see legend) and enclosed bubbles indicate significant pathway enrichment. In heatmap: genes were clustered according to their expression pattern (Euclidean distance) and column clustering groups samples based on gene expression similarity. Color scale indicates the expression levels (yellow, low expression; blue, high expression).

alkaline salinity, three sets of DEGs were established (Fig. 2D): the 345 DEGs found in response to *neuSAL* but not to *alkSAL* were referred to as *onlyNEUSAL* set (Dataset B5), the 3585 DEGs altered under *alkSAL* but not under *neuSAL* were referred to as *onlyALKSAL* set (Dataset B6), and the 1219 shared DEGs under both *neuSAL* and *alkSAL* treatments were referred to as *coreSAL* set (Dataset B7). The number of DEGs obtained among treatments shows that the stress imposed on plants by alkaline salinity is distinct from that imposed by neutral salinity (Guo et al., 2010). In all sets, more than 90 % of DEGs shared expression trend (upregulation or downregulation) among all demes. Studies by others assessing *Arabidopsis* response to complex stresses have described antagonistic expression trends for only 5–10 % of transcripts

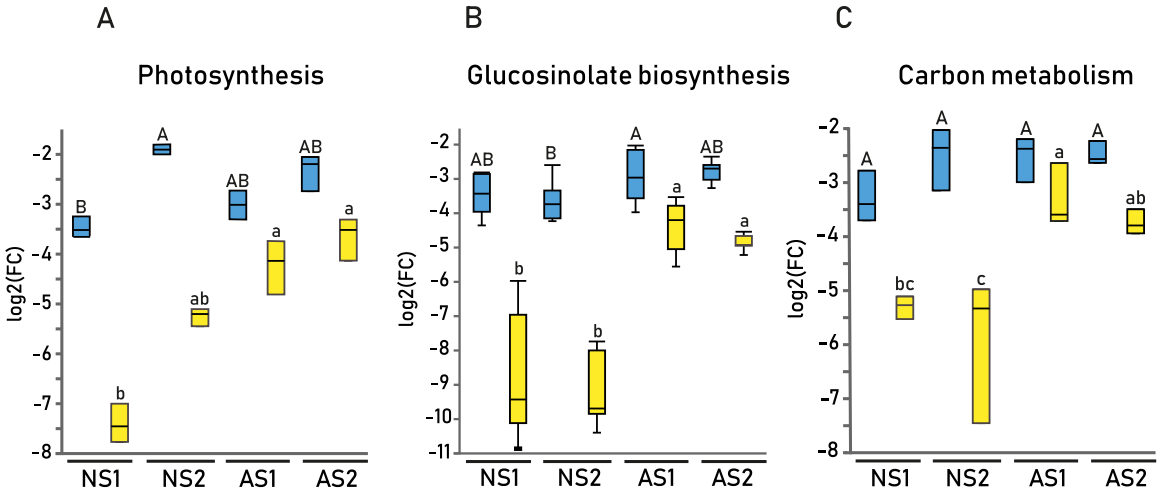


**Fig. 4. Dissection on significantly enriched pathways from *coreSAL* downregulated DEGs under neutral salinity (*neuSAL* in blue) and alkaline salinity (*alkSAL* in yellow) treatments.** Expression levels [mean ± SE log2(FC)] of DEGs from the **(A)** "Photosynthesis" (n=8), **(B)** "Glucosinolate biosynthesis" (n=9) and **(C)** "Carbon metabolism" (n=5) pathways in each deme and treatment. Letters indicate significant differences in mean expression values among demes under *neuSAL* (capital) and *alkSAL* (lower case) (Tukey's HSD, adj. *p*-value < 0.05).

(Rasmussen et al., 2013), which supports our observations.

### 3.4. Enhanced inhibition of photosynthesis and carbon metabolism genes in carbonate-sensitive demes under alkSAL

KEGG pathway analysis was performed in *onlyNEUSAL*, *onlyALKSAL* and *coreSAL* DEGs to identify metabolic pathways significantly enriched (*q*-value < 0.05) in general salinity stress responses. The *onlyNEUSAL*, *onlyALKSAL* and *coreSAL* enriched pathways are listed in Dataset B8 – B10 and represented in Fig. 3. The expression levels of DEGs contained in significantly enriched metabolic pathways were compared between the NS and AS demes to detect the presence of genotype-dependent responses to alkaline salinity at the transcriptomic level. In the *coreSAL* and *onlyalkSAL* sets, the most significantly enriched pathways contained down-regulated transcripts and were 'Photosynthesis' and 'Photosynthesis antenna proteins' (Fig. 3). NS demes, especially NS1, showed a significant repression of photosynthetic enzymes and subunits of the PS antenna system (an average of 1.5 and 1.8 times more downregulation than AS1 and AS2, respectively) (Fig. 4A). This supports the enhanced inhibition of photosynthesis found in NS demes, specially NS1, when compared to AS demes under *alkSAL*. The up-regulation of subunits H of photosystem I reaction center is a characteristic trait of halophytes (Hao et al., 2020), whereas the inhibition in the expression of photosynthesis related transcripts has been found to correlate with increased salt sensitivity (Guo et al., 2017; Jing et al., 2019).

DEGs from "glucosinolate biosynthesis" and a DEG subset from "carbon metabolism" displayed an average of 1.7-fold more down-regulation in NS1 and NS2 compared to AS1 and AS2 under *alkSAL* (Fig. 4B&C). More specifically, two Ribulose Biphosphate Carboxylase Subunits (*RBNS1–2B*), a Hydroxypyruvate Reductase (*HPR*) and a Fumarase (*FUM2*) comprised the DEG subset from "carbon metabolism", sharing an expression pattern with the glucosinolate pathway in NS demes. Finally, the inhibition of the transcripts of *α-CA* and *β-CA* (Carbonic Anhydrases) (*α-CA1*, *α-CA2*, *β-CA1*, *β-CA2* and *β-CA4*), and glutamine synthetases 1;4 (*GLN1;4*) and 2 (*GS*) family proteins comprised the last enriched down-regulated set. From these, *βCA-1* (At3G01500) and *α-CA1* (At3G52720) displayed 1.7-fold stronger inhibition in NS1 compared to AS1 and AS2 under *alkSAL* (Figure A3). *βCA-1* is reported to regulate $CO_2$ controlled stomatal movements in guard cells together with *βCA4* (AT1G70410). Previous studies reported *βCA4* reduction in NS1 under bicarbonate conditions (Pérez-Martín, 2021), and a *βca1βca4* mutant exposed to $NaHCO_3$ showed reduced photosynthetic efficiency ($F_v/F_m$) and increased total ion leakage (as reporter for cell death) (Dąbrowska-Bronk et al., 2016). *α-CA1* belongs to the *α-CA* family and is involved in the transformation of $HCO_3^-$ to $CO_2$ in the chloroplast stroma to supply it at the active site of Rubisco (Burén, 2010). Considering the high demand for Fe cofactors by photosynthetic enzymes (Kroh and Pilon, 2020), the above results point to a defective Fe use efficiency in NS demes under *alkSAL* (especially NS1), exacerbating photosynthetic inhibition. This would result in the observed unbalance in carbon fixation and metabolism in NS1 and NS2. In such a scenario, the stronger downregulation of both enzymes catalyzing entrance reactions into major pathways of the plant primary metabolism and chloroplast carbonic anhydrases (*β-CA1* and *α-CA1*) in NS demes under *alkSAL* is consistent with their reduced photosynthesis efficiency ($F_v/F_m$ values). Moreover, stronger downregulation of transcripts from photosynthesis and carbon fixation and metabolism (*RBNS1–2B*, *HPR* and *FUM2*) ultimately compromises their total energy investment in secondary metabolism, leading to the downregulation of all transcripts involved in glucosinolate biosynthesis. Likewise, the results confirm that a significant inhibition of glucosinolate signaling in NS demes is caused in an alkalinity-specific manner, probably due to the lower availability of ferrous ions (Fahey et al., 2001; Wittstock et al., 2002). Contrastingly, bicarbonate tolerance in *A. thaliana* is specifically related to the upregulation of glucosinolate biosynthesis related genes (Pérez-Martín et al., 2021).

### 3.5. Salinity-triggered phytohormone responses are alkalinity-dependent

In *onlyNEUSAL*, the most significantly enriched pathway was "Phytohormone signaling" and it was mainly comprised by down-regulated transcripts (Fig. 3). To identify activation or repression patterns in phytohormone signaling pathways among treatments, the expression levels of phytohormone-responsive genes were analyzed in *neuSAL* and *alkSAL* (*q*-value < 0.05; Student *t*-Test) (Fig. 5A; Dataset B11). In parallel, endogenous phytohormones were quantified in the leaf tissue of the four demes under *control*, *neuSAL* and *alkSAL* treatments to get an insight of the signaling mechanisms underlying differential phytohormone profiles (Fig. 6). The concentrations of the analyzed phytohormones can be found in Dataset B12.

Higher inhibition of auxin-responsive genes (*SAUR*s and, *Aux/IAA*s) and JA-responsive genes (*LOX*, *MYC*s) was observed after 2 weeks of exposure to *alkSAL* compared to *neuSAL* (Fig. 5B-C). In contrast, a significant elicitation (*p*-value ≤ 0.01, Student's *t*-Test) of IAA, and JA was

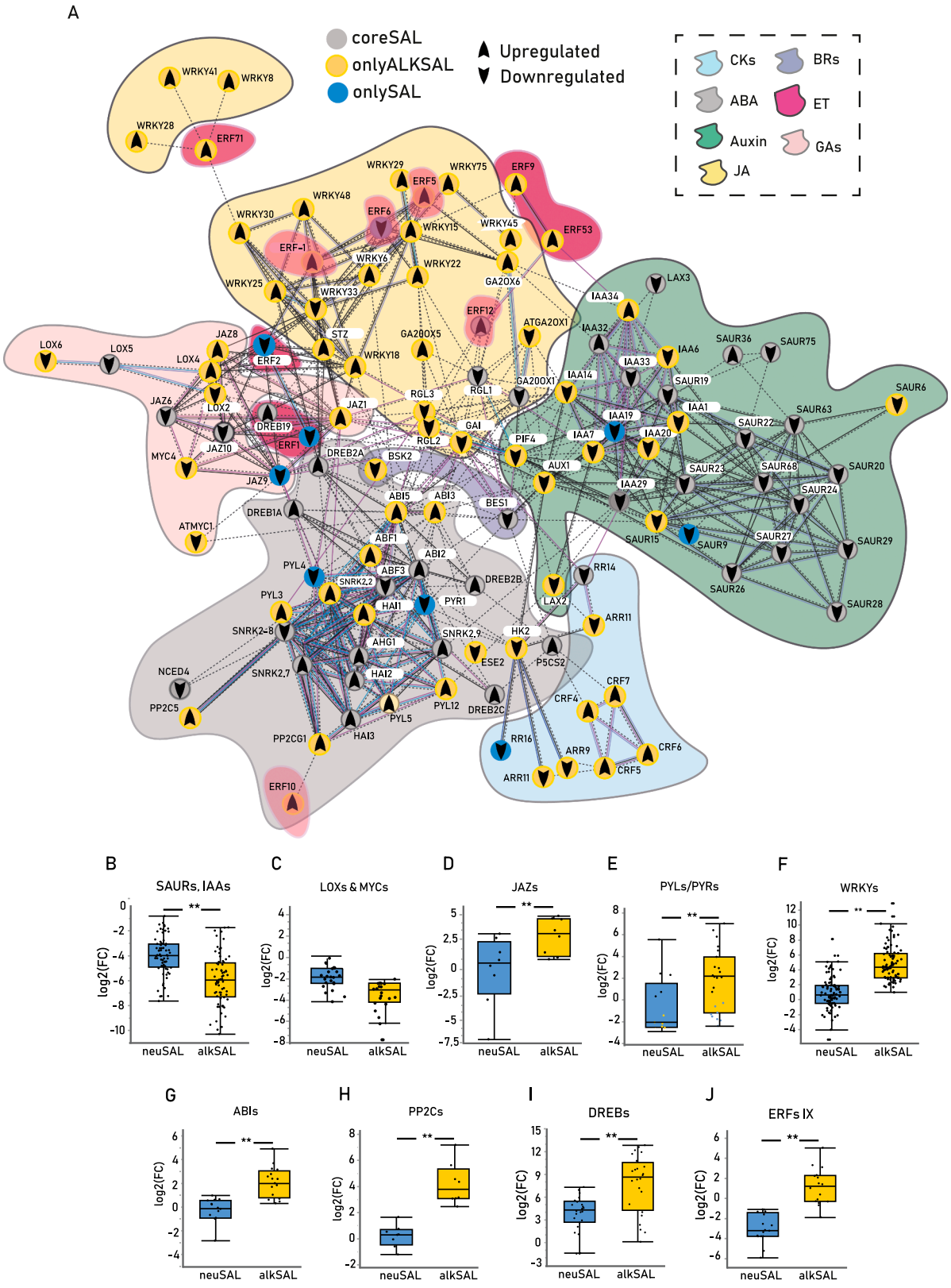


**Fig. 5. Global overview of phytohormone signaling dynamics. (A)** Protein-protein interaction (PPI) network of the analyzed DEGs involved in phytohormone signaling based on the STRING online database (https://string-db.org/). Nodes are color-coded according to each DEGs subset, arrows inside nodules indicate expression trend and colored surrounding areas distinguish between different hormone classes (see legends). Expression levels [mean ± SE log2(FC)] of DEGs from **(B)** SAURs & IAAs (n=56), **(C)** LOXs/MYCs (n=20), **(D)** JAZs (n=8), **(E)** PYLs/PYRs (n=23), **(F)** WRKYs (n=44), **(G)** ABIs (n=16), **(H)** PP2Cs (n=8), **(I)** DREBs (n=24) and **(J)** IX clade ERFs (n=12), in all demes among treatments. Asterisks indicate significant differences in mean expression values among treatments (Student t-test, adj. p-value < 0.05; *: adj. p-value < 0.05; **: adj. p-value < 0.01). Neutral salinity: *neuSAL*; alkaline salinity: *alkSAL*.

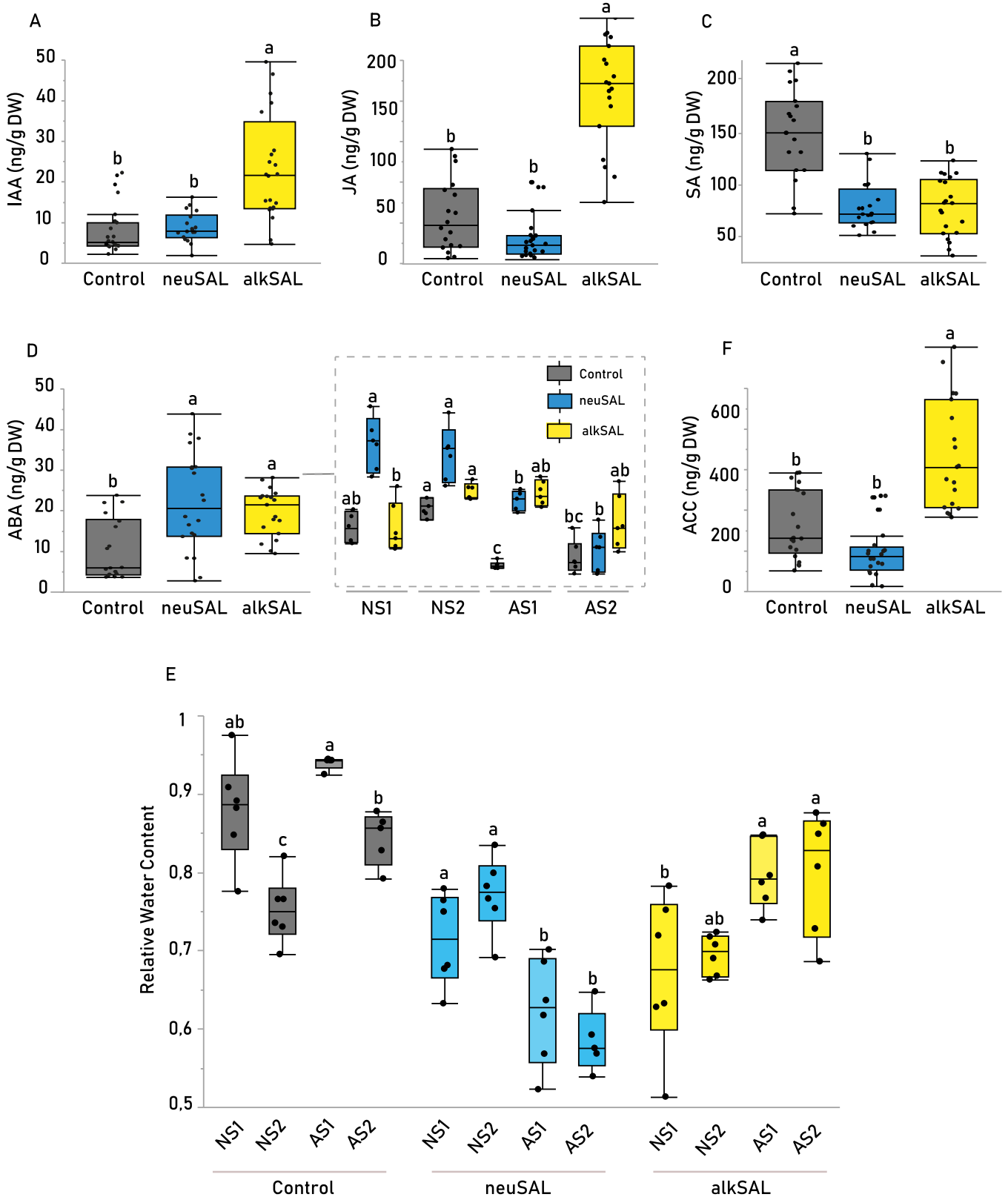


**Fig. 6. Endogenous phytohormone and relative water content in *A. thaliana* demes under control (C), neutral (*neuSAL*) and alkaline (*alkSAL*) salinity.** Mean (ng $g^{-1}$ DW) ± SE of relative **(A)** Indole acetic acid (IAA), **(B)** Jasmonic Acid (JA), **(C)** Salicylic Acid (SA), **(D)** Abscisic Acid (ABA) and **(F)** 1-Aminocyclopropane-1-carboxylic acid (ACC). Each dot represents a biological replicate (n=6), and treatments are color-coded (see legend). Zoomed boxplots show relative phytohormone concentration for each deme. **(E)** Relative water content of each deme under control, neuSAL and alkSAL. Mean values with different letters indicate significant differences (Tukey's HSD, adj. p-value < 0.05). Plants were grown in potting mix soil and irrigated with C (0.5-Hoagland, pH 5.9), neuSAL (100 mM NaCl, pH 5.9) or alkSAL (85 mM NaCl, 15 mM $NaHCO_3$, pH 8.3) for 2 weeks.

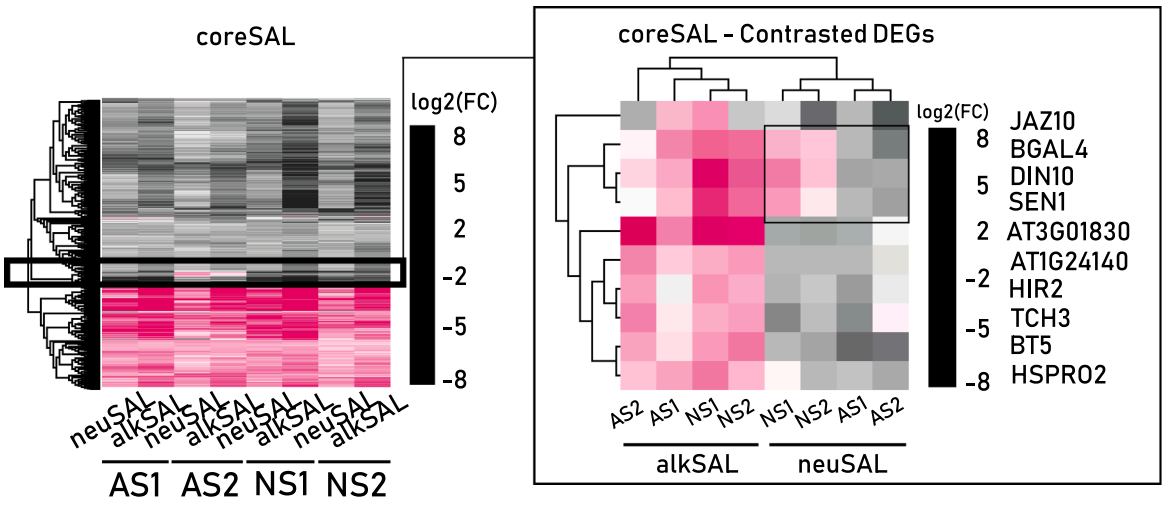


**Fig. 7. Characterization of the coreSAL DEGs set.** DEGs were filtered at log fold change (LFC > 2, LFC < −2), and *q*-value (FDR-adjusted *p*-value) < 0.05. Heat map showing the expression profile of coreSAL DEGs (1219 genes) for each deme between neutral and alkaline salinity when compared to control (neuSAL/C; alkSAL/C). Genes were clustered according to their expression pattern (Euclidean distance). In frame, heatmap showing the expression profiles of coreSAL DEGs with contrasted expression trends among salinity types and/or demes. The color scale indicates the expression levels (grey, low expression; pink, high expression). Genes were clustered according to their expression pattern (Euclidean distance), while column clustering groups samples based on gene expression similarity.

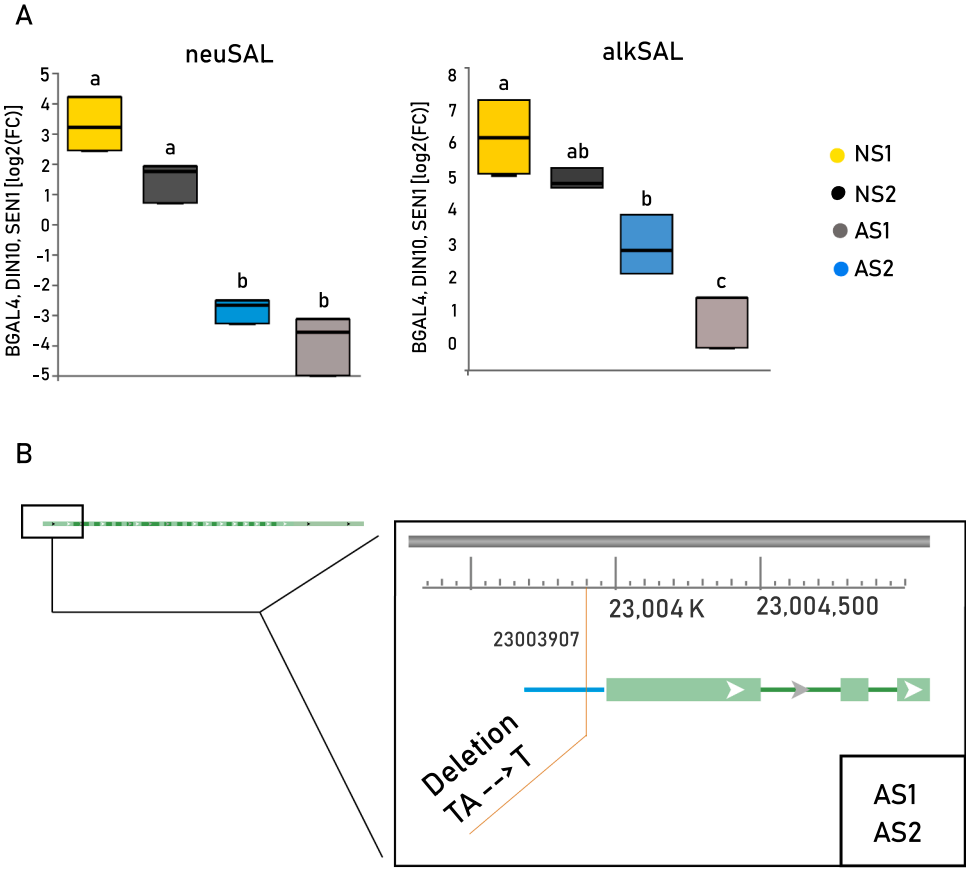


**Fig. 8. Characterization of *BGAL4* expression and sequence variation in *A. thaliana* demes. (A)** Expression levels [mean ± SE log2(FC)] of *BGAL4, DIN10* and *SEN1* in each deme (n=9) and treatment. Letters indicate significant differences in mean expression values among demes (Tukey's HSD, adj. *p*-value < 0.05). NS1 (yellow), NS2 (black), AS1 (blue), and AS2 (grey). **(B)** SNP polymorphisms surrounding the *BGAL4* locus. Triangles: candidate SNPs position. Amino acid change is indicated below each SNP. Gene orientation is indicated with an arrow on the right. Exons are indicated with boxes and introns with lines connecting them. Chromosome positions are indicated at the top left (picture from https://www.arabidopsis.org/index.jsp). Reference and alternative allele nucleotide changes, variant type and deme bearing the SNP can be found in Fig. A4.

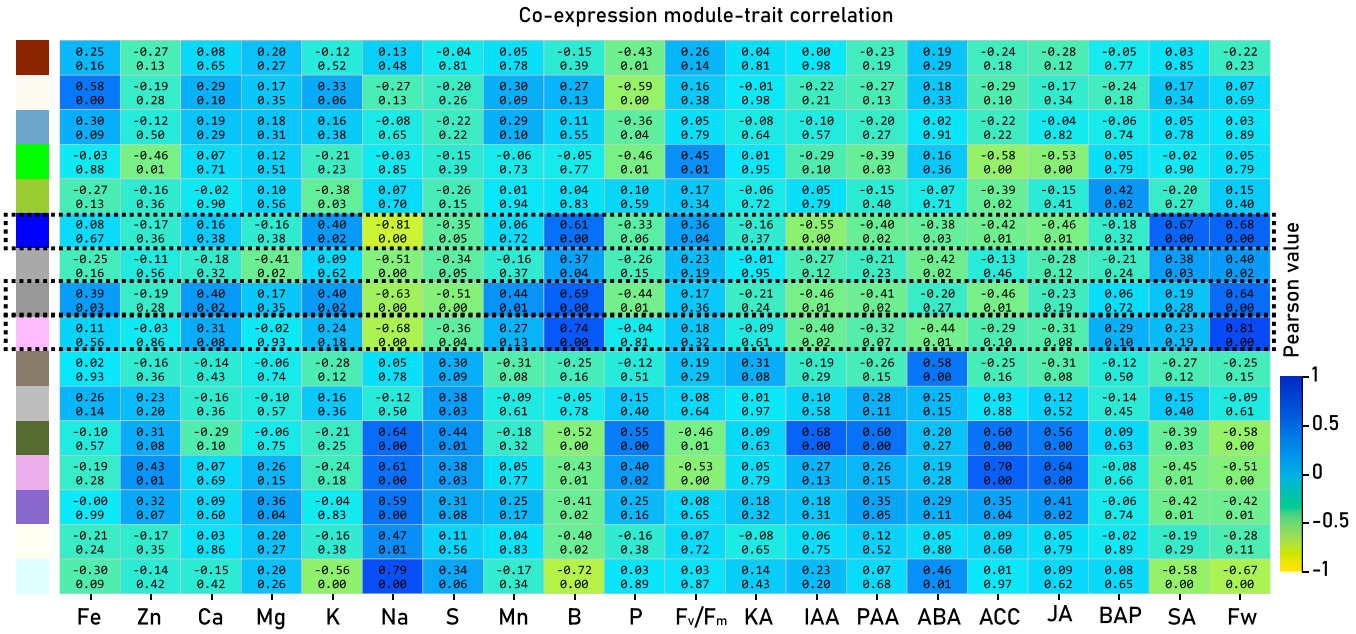


**Fig. 9. WGCNA analysis.** Relationships of co-expression modules and analyzed physiological traits. Each row in the table corresponds to a co-expression module, and each column to a trait. Numbers in the matrix report the correlations of the corresponding module genes and each trait, with the p values below the correlations in parentheses. The table is color coded by correlation according to the color legend.

observed under *alkSAL* compared to *control* and *neuSAL* treatment (Fig. 6A-B). Leaf SA decreased and ABA increased under both *neuSAL* and *alkSAL* (Fig. 6C-D), which supports previous observations on ABA-SA and JA-SA antagonistic signaling (Kazan and Manners, 2012; Moeder et al., 2010). The downregulation of *SAURs* and *LOX/MYCs* during the late phase of the plant salinity response is consistent with a targeted protein degradation following the observed auxin and JA accumulation. *SAURs* reduced expression under *alkSAL* suggest further repression of auxin signaling mediated by the presence of JA and ABA rather than the removal of the inducer (IAA) (Markakis et al., 2013) and depicts an ABA/IAA-dependent regulation mechanism of the PM $H^+$-ATPase activity under alkaline salinity (Li et al., 2022). Besides, the exclusive induction of repressors of the JA pathway (*JAZs*), targeting MYCS repression by *alkSAL* was accompanied by significant upregulation of ABA receptors (*PYLs*), ABA responsive genes (*WRKY*, *ABIs*) and other ABA-dependent MAPK phosphatases (*PP2CS*) (Fig. 5D-H). This supports an antagonistic interaction between ABA and JA signaling pathways modulating stress-responsive gene expression (Anderson et al., 2004; Kazan and Manners, 2013; Sah et al., 2016). It also suggests a negative regulatory feedback loop occurring after prolonged exposure to alkaline salinity, to turn off the transcriptional reprogramming caused by the accumulation of JA under *alkSAL,* and to minimize JA-induced inplant growth inhibition in an attempt of acclimation (Riemann et al., 2015). In turn, the stimulation of ABA signaling and accumulation is likely mediated by *WRKYs* (Hussain et al., 2021), which remained active after 2 weeks of *neuSAL* and *alkSAL* treatment. Among them, enhancers of osmotic, ROS and hormone signaling pathways under salinity stress have been recently reported (Price et al., 2022).

However, the studied demes exhibited an origin-dependent accumulation profile for ABA under *neuSAL* and not under *alkSAL*: the NS demes,NS1 and NS2 displayed higher ABA accumulation compared to AS1 and AS2 (Fig. 6D). Salinity-induced ABA biosynthesis is well documented, causing stomatal closure, reducing stomatal conductance and water consumption, and promoting overall plant tolerance to salinity (Lovelli et al., 2012). Plant relative water content (RWC) was determined to test if ABA accumulation contributes to the enhanced response of locally adapted demes to *neuSAL* conditions by increasing their water use efficiency (Cardoso et al., 2020; Chen et al., 2022). In fact, ABA concentrations in NS demes under *neuSAL* was correlated with higher plant relative water content (RWC) (Fig. 6E; Dataset B13), suggesting that ABA enhances leaf salt resistance by improving the plant water status through reduced stomatal conductance.

Finally, *DREBs* (Dehydration responsive element binding) showed sustained activation under both *neuSAL* and *alkSAL,* with significantly higher transcript expression in *alkSAL* (Fig. 5I). Most DREBs regulate the expression of multiple stress-inducible genes and play pivotal roles in the plant abiotic stress response. All identified *DREBs* showed strong upregulated after 2-week exposure to both *neuSAL* and *alkSAL.* Among them, we found *DREB1A* and *DREB2C* which are reported as two of the *DREBs* that contain the most types of abiotic stress-related motifs in the promoter region (Xie et al., 2019). The sustained upregulation of *DREBs* in the *coreSAL* gene set under long-term salinity exposure provides additional evidence that *DREBs* form a central network to control the plant salinity response also in the late stage (Sazegari et al., 2015). Contrarily, sustained upregulation of twelve DEGs of another subfamily of *AP2/ERF* transcription factors, *ERF-IX*, seems to be required solely by alkaline salinity stress (Fig. 5J) and is associated with significant ACC accumulation in the plant under *alkSAL* (Fig. 6F) (Wang et al., 2022).

Overall, greater alteration in the plant transcriptome caused by alkaline salinity leads to more extensive rearrangement in the *alkSAL* phytohormonal signaling network. In this regard, transcript inhibition for protein turnover seems to be a regulation mechanism for phytohormone signaling pathways such as auxin and JA under *alkSAL,* and ABA under *neuSAL* (McClellan and Chang, 2008), the latter being an adaptive mechanism to improve plant water use efficiency. The implication of the differential mechanisms of auxin and ABA regulation for proton extrusion, through the activation of $H^+$-ATPase by the inhibition of PP2C proteins, should be further addressed as it is an essential Fe-deficiency plant response (Sun et al., 2020; Spartz et al., 2014).

### *3.6. A reduced coreSAL DEG subset orchestrates contrasted plant response to neuSAL and alkSAL*

All shared DEGs displaying opposite expression trends between neuSAL and alkSAL were analyzed to seek contrasted transcriptomic responses potentially driving differential performance under each

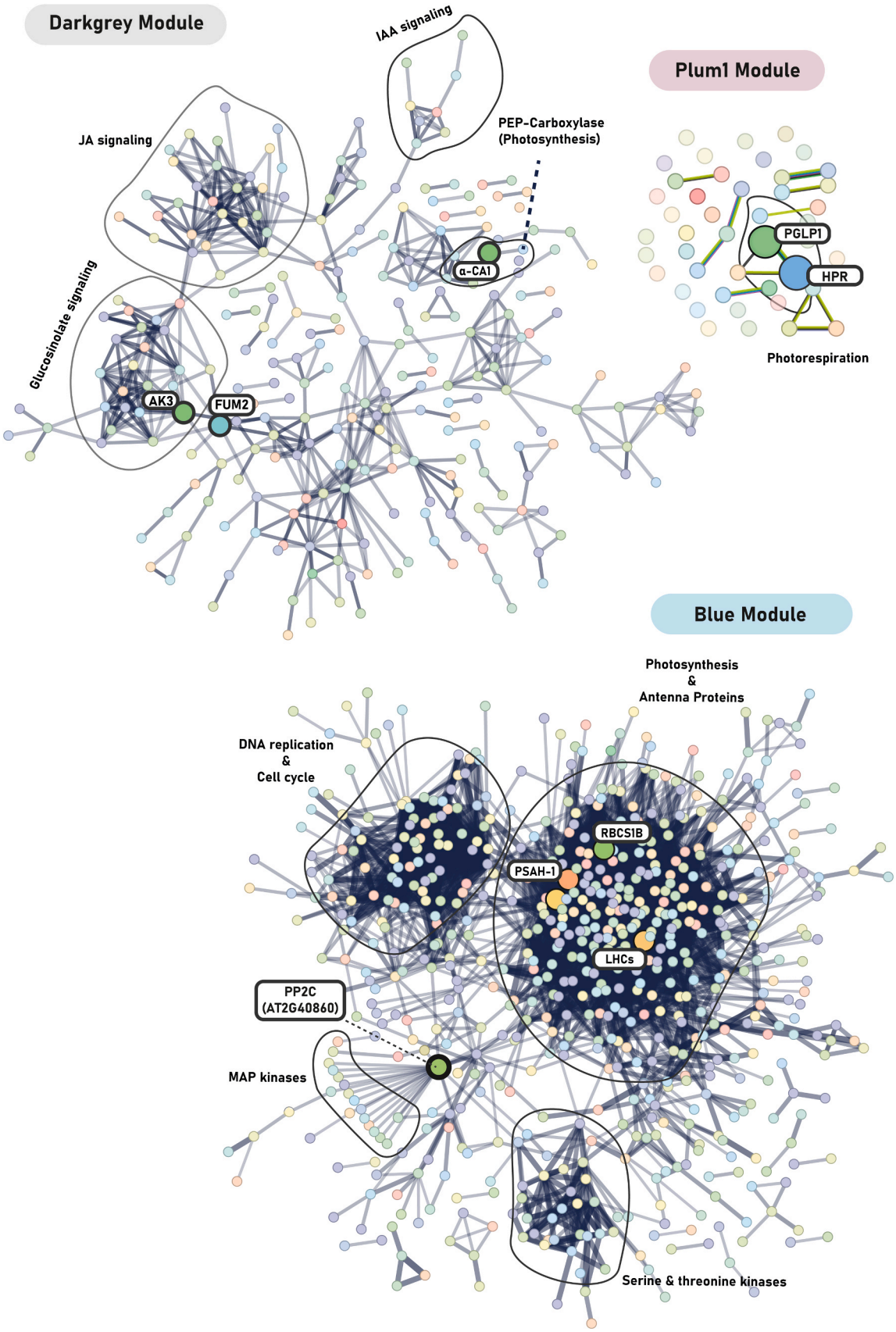


**Fig. 10. Overview of WGCNA co-expression modules significantly correlating to alkaline salinity tolerance traits.** Protein-protein interaction (PPI) network of all DEGs comprised in darkgrey, plum1 and blue WGCNA co-expression modules, based on the STRING online database (https://string-db.org/). Proposed candidates identified in each module and appearing on each PPI Network are indicated, and main signaling pathways enriched per module encircled.

salinity type (Fig. 7). *BGAL4* (AT5G56870), *DIN10* (AT5G20250) and *SEN1* (AT4G35770) exhibited contrasting expression trends among AS1 and AS2 (down-regulated) and NS1 and NS2 (up-regulated) under *neuSAL* (Fig. 8A). This suggests that activation of *BGAL4*, *DIN10* and/or *SEN1* is advantageous under *neuSAL* but not under *alkSAL*. The genomic sequences of *BGAL4*, *DIN10* and *SEN1* in the 4 study demes were extracted from the Whole Genome Sequencing (WGS) data of the Catalan demes' germplasm (Busoms et al., 2018) to identify variants likely causal of the contrasted expression trends in the studied demes under *neuSAL* and *alkSAL* (Figure A4; Dataset B14). Indeed, a SNP located just 4 bp upstream of the 5'UTR was identified in the *BGAL4* promoter. This SNP differentiated alkaline salinity tolerant from sensitive demes and was consistent for all replicates of each deme (Fig. 8B).

*BGAL4* encodes a glycosyl hydrolase regulated by SNF1-related Kinase 1 (*SnRK1*), a kinase involved in key plant stress responses (Peixoto et al., 2021). The degradation of structural polysaccharides in plant cell wall by cell wall remodeling enzymes like BGAL4 is part of the stress-regulated cell wall rearrangement (Moneo-Sánchez et al., 2016). A study comparing *A. thaliana* Wild Type vs salt-tolerant mutant roots exposed to NaCl stress reported increased expression of glycosyl hydrolases in the salt-tolerant mutant root, which was hypothesized to increase its potential of salt resistance (Guo et al., 2014). In contrast, β-galactosidases have been reported to dramatically decrease enzymatic activity at high pH and to have pH optima ranging from 3.5 to 5.0 (Ross et al., 1994; Smith and Gross, 2000; Kotake et al., 2005; Hussien and Doosh, 2021). Thus, enhanced upregulation of *BGAL4* in NS1 and NS2 could indicate greater activation of plant energy management functions in NS demes under *neuSAL* but not under *alkSAL* Transcription factor binding is the strongest contributor to variation in mRNA levels (Pai et al., 2015). This might be the case for *BGAL4*, where the SNP change in the promoter region of AS1 and AS2 could contain cis-regulatory elements responsible for its consistently lower expression. To confirm this hypothesis, enzymatic activity assays on plant-derived cell wall substrates should be performed across a pH range of pH 4–10 by using the recombinant BGAL4 (Ahn et al., 2007). Besides, Arabidopsis *BGAL4* knockdown and overexpression lines should be screened under *neuSAL* and *alkSAL* to validate the involvement of *BGAL4* modulation in the tolerance to differential salinity types.

### *3.7. Weighted Correlation Network Analysis tag the significant candidate genes involved in favorable responses to both salinity types*

To combine transcriptomic and physiological datasets and detect possible correlations between genes determining traits of interest, all DEGs detected in each deme under *neuSAL* and *alkSAL* treatment were retained for WGCNA unsigned co-expression network analysis. This involved a total of 11432 DEGs (11 K WGCNA hereafter). The soft threshold power of 7 ($\beta = 7$) was selected according to the preconditions of the approximate scale-free topology (Figure A5). WGCNA analysis identified sixteen distinct co-expression modules that were assigned to different colors (Figs. A6–8). The module-trait correlation matrix obtained displayed two major contrasted patterns defined by correlation trends in 2 main traits: leaf $Na^+$ and relative rosette biomass (Fig. 9). Besides, most co-expression modules that negatively correlated with leaf $Na^+$ and positively correlated with sample biomass also showed a positive correlation with other favorable plant traits for abiotic stress tolerance, such as leaf $K^+$ concentration and $F_v/F_m$ values (Fig. 9).

The DEGs comprised in the significantly enriched pathways of each module were compared with the stablished set of DEGs from *coreSAL*, *onlyNEUSAL* and *onlyALKSAL*. The modules showing a significant negative correlation with $Na^+$ and a positive correlation with $K^+$ or FW were picked up and compared with the *coreSAL* DEGs. "Photosynthesis and Photosynthesis Antenna Proteins", from the blue module, and "Glucosinolate Biosynthesis", from the grey module, contained 74 % and 66 % of the DEGs included at the *coreSAL* set, respectively (Dataset B15).The results confirmed that DEGs selection criteria used for transcriptome analysis accurately reflected the behavior of the entire data set (Fig. 10). These findings provide an important reference for understanding the responses and adaptations to neutral and alkaline salinity in glycophytic plants.

## 4. Conclusions

By means of an integrative physiological, ionomic and transcriptomic approach, convergent and divergent biological pathways that confer shared and exclusive responses to neutral (*neuSAL*) and alkaline salinity (*alkSAL*) have been revealed in natural populations of *Arabidopsis thaliana*. This integrative view is summarized in Figure A9. Dissection of down-regulated transcripts in the *coreSAL* set confirms that neutral salinity tolerance does not confer advantageous features under alkaline salinity conditions and points to key genes involved in the photorespiratory cycle, organic acid accumulation, and secondary metabolic processes like glucosinolate biosynthesis as targets for alkaline salinity resistance breeding. In this concern, when facing alkaline salinity stress, it is essential to increase the efficiency of internal Fe use to maintain the photosynthesis rate and increase the accumulation of Ca and K, to reduce leaf Na:K and Na:Ca ratios. Moreover, enhanced activation of ABA-dependent signaling is highlighted as a key trait for plant performance under *alkSAL*, likely by PYL/PYRs binding to PP2CS and consequent activation of $H^+$ATP-ase activity, allowing apoplastic acidification. In turn, the accumulation and sustained signaling of ABA is shown exclusively in the NS demes, NS1 and NS2 tolerant to *neuSAL and* is proposed as an adaptive strategy through the improvement of plant water status. Screening results of DEGs with contrasting expression profiles among demes indicate that a smart regulation of *BGAL4*, a cell wall and tonoplast hydrolase, is key to tolerate alkaline salinity. A SNP detected in the 5'UTR of AS1 and AS2 is proposed as a candidate for the attenuation of *BGAL4* expression under alkaline salinity, favoring the prioritization of compounds more suitable in alkaline conditions and optimizing the plant energy budget.

## Author Statement

MJ-A, SB, LP-M, AG, ML and CP conceived the study. MJ-A and LP-M performed the laboratory experiments. MJ-A, LP-M, GE-O and AL-V performed data analysis. MJ-A, SB, and CP wrote the manuscript with inputs from all coauthors. All the authors gave final approval for publication.

## CRediT authorship contribution statement

**Álvaro López-Valiñas:** Formal analysis, Data curation. **Antoni Garcia:** Writing – review & editing, Supervision. **Laura Pérez-Martín:** Writing – original draft, Methodology, Data curation. **Glòria Escolà:** Formal analysis, Data curation. **Maria Jose Almira-Casellas:** Writing – review & editing, Writing – original draft, Validation, Methodology, Investigation, Formal analysis, Conceptualization. **Silvia Busoms:** Writing – review & editing, Supervision, Investigation, Data curation, Conceptualization. **Charlotte Poschenrieder:** Writing – review & editing, Supervision, Investigation, Conceptualization. **Mercè Llugany:** Writing – review & editing, Supervision, Conceptualization.

## Declaration of Competing Interest

The authors declare the following financial interests/personal relationships which may be considered as potential competing interests: Charlotte Poschenrieder reports financial support was provided by Ministry of Science Technology and Innovations. If there are other authors, they declare that they have no known competing financial interests or personal relationships that could have appeared to influence the work reported in this paper.

## Acknowledgements

Special thanks to Rosa Padilla for processing ICP and HPLC samples and to Olga Jáuregui from Serveis Científico-Tècnics of the University of Barcelona. This research was supported by the Spanish Ministry of Science and Innovation (MICINN) (PID 2019 104000 RB I00).

*Declaration of interest statement*

The authors declare that they have no conflict of interest.

## Appendix A. Supporting information

Supplementary data associated with this article can be found in the online version at doi:10.1016/j.envexpbot.2024.105982.

## References

Ahn, Y.O., Zheng, M., Bevan, D.R., Esen, A., Shiu, S.H., Benson, J., Shih, M.C., 2007. Functional genomic analysis of *Arabidopsis thaliana* glycoside hydrolase family 35. Phytochemistry 68 (11), 1510–1520. https://doi.org/10.1016/j.phytochem.2007.03.021.

An, Y.M., Song, L.L., Liu, Y.R., Shu, Y.J., Guo, C.H., 2016. De novo transcriptional analysis of alfalfa in response to saline-alkaline stress. Front. Plant Sci. 7, 931. https://doi.org/10.3389/fpls.2016.00931.

Anderson, J.P., Badruzsaufari, E., Schenk, P.M., Manners, J.M., Desmond, O.J., Ehlert, C., Kazan, K., 2004. Antagonistic interaction between abscisic acid and jasmonate-ethylene signaling pathways modulates defense gene expression and disease resistance in Arabidopsis. Plant Cell 16 (12), 3460–3479. https://doi.org/10.1105/tAS.104.025833.

Bomblies, K., Yant, L., Laitinen, R.A., Kim, S.T., Hollister, J.D., Warthmann, N., Weigel, D., 2010. Local-scale patterns of genetic variability, outcrossing, and spatial structure in natural stands of *Arabidopsis thaliana*. PLoS Genet. *6* (*3*), e1000890. https://doi.org/10.1371/journal.pgen.1000890.

Burén, S., 2010. *Targeting and function of CAH1: Characterization of a novel protein pathway to the plant cell chloroplast* (Doctoral dissertation, Institutionen för fysiologisk botanik, Umeå universitet). diva, id: diva2, 284338.

Busoms, S., Paajanen, P., Marburger, S., Bray, S., Huang, X.Y., Poschenrieder, C., Salt, D. E., 2018. Fluctuating selection on migrant adaptive sodium transporter alleles in coastal *Arabidopsis thaliana*. Proc. Natl. Acad. Sci. *115* (*52*), E12443–E12452. https://doi.org/10.1073/pnas.1816964115.

Busoms, S., Pérez-Martín, L., Terés, J., Huag, X.-Y., Yant, L., Tolrà, R., Salt, D.E., Poschenrieder, C., 2023. Combined genomics to discover genes associated with tolerance to doil carbonate. *Plant Cell and Environment*, 46, 3986–3998.

Busoms, S., Teres, J., Huang, X.Y., Bomblies, K., Danku, J., Douglas, A., Salt, D.E., 2015. Salinity is an agent of divergent selection driving local adaptation of Arabidopsis to coastal habitats. Plant Physiol. *168* (*3*), 915–929. https://doi.org/10.1104/pp.15.00427.

Cardoso, A.A., Gori, A., Da-Silva, C.J., Brunetti, C., 2020. Abscisic acid biosynthesis and signaling in plants: Key targets to improve water use efficiency and drought tolerance. Appl. Sci. *10* (18), 6322. https://doi.org/10.3390/app10186322.

Chen, G., Zheng, D., Feng, N., Zhou, H., Mu, D., Zhao, L., Huang, A., 2022. Physiological mechanisms of ABA-induced salinity tolerance in leaves and roots of rice. Sci. Rep. *12* (*1*), 8228. https://doi.org/10.1038/s41598-022-11408-0.

Cheng, N.H., Liu, J.Z., Nelson, R.S., Hirschi, K.D., 2004. Characterization of CXIP4, a novel Arabidopsis protein that activates the H+/Ca2+ antiporter, CAX1. FEBS Lett. *559* (1-3), 99–106. https://doi.org/10.1016/S0014-5793(04)00036-5.

Dąbrowska-Bronk, J., Komar, D.N., Rusaczonek, A., Kozłowska-Makulska, A., Szechyńska-Hebda, M., Karpiński, S., 2016. β-carbonic anhydrases and carbonic ions uptake positively influence Arabidopsis photosynthesis, oxidative stress tolerance and growth in light dependent manner. J. Plant Physiol. *203*, 44–54. https://doi.org/10.1016/j.jplph.2016.05.013.

Delatorre, C., Rodríguez, A., Rodríguez, L., Majada, J.P., Ordás, R.J., Feito, I., 2017. Hormonal profiling: development of a simple method to extract and quantify phytohormones in complex matrices by UHPLC–MS/MS. J. Chromatogr. B 1040, 239–249.

Eroglu, S., Meier, B., von Wirén, N., Peiter, E., 2016. The vacuolar manganese transporter MTP8 determines tolerance to iron deficiency-induced chlorosis in Arabidopsis. Plant Physiol. 170 (2), 1030–1045.

Fahey, J.W., Zalcmann, A.T., Talalay, P., 2001. The chemical diversity and distribution of glucosinolates and isothiocyanates among plants. Phytochemistry *56* (1), 5–51. https://doi.org/10.1016/S0031-9422(00)00316-2.

Fang, S., Hou, X., Liang, X., 2021. Response mechanisms of plants under saline-alkali stress. Front. Plant Sci. 12, 667458. https://doi.org/10.3389/fpls.2021.667458.

Garg, N., Pandey, R., 2015. Effectiveness of native and exotic arbuscular mycorrhizal fungi on nutrient uptake and ion homeostasis in salt-stressed *Cajanus cajan* L. (Millsp.) genotypes. Mycorrhiza *25* (3), 165–180. https://doi.org/10.1007/s00572-014-0600-9.

Guo, M., Li, H., Li, L., Cheng, X., Gao, W., Xu, Y., Liu, X., 2014. Comparative proteomic analysis of Arabidopsis thaliana roots between wild type and its salt-tolerant mutant. J. Plant Interact. *9* (1), 330–337. https://doi.org/10.1080/17429145.2013.833653.

Guo, R., Shi, L., Ding, X., Hu, Y., Tian, S., Yan, D., Yang, Y., 2010. Effects of saline and alkaline stress on germination, seedling growth, and ion balance in wheat. Agron. J. 102 (4), 1252–1260. https://doi.org/10.2134/agronj2010.0022.

Guo, R., Shi, L., Yan, C., Zhong, X., Gu, F., Liu, Q., Li, H., 2017. Ionomic and metabolic responses to neutral salt or alkaline salt stresses in maize (*Zea mays* L.) seedlings. BMC Plant Biol. *17* (1), 1–13. https://doi.org/10.1186/s12870-017-0994-6.

Hao, X., Li, J., Gao, S., Tuerxun, Z., Chang, X., Hu, W., Huang, Q., 2020. SsPsaH, a H subunit of the photosystem I reaction center of *Suaeda salsa*, confers the capacity of osmotic adjustment in tobacco. Genes GenomiNS *42* (12), 1455–1465. https://doi.org/10.1007/s13258-020-00970-4.

Hussain, Q., Asim, M., Zhang, R., Khan, R., Farooq, S., Wu, J., 2021. Transcription factors interact with ABA through gene expression and signaling pathways to mitigate drought and salinity stress. Biomolecules *11* (*8*), 1159. https://doi.org/10.3390/biom11081159.

Hussien, S.A., Doosh, K., 2021. Extraction, Purification and Characterization of β-Galactosidase from Tomato (*Lycopersicom esculentum*). In: In *IOP Conference Series: Earth and Environmental Science*, Vol. 761. IOP Publishing, 012123. https://doi.org/10.1088/1755-1315/761/1/012123.

Jin, T., An, J., Xu, H., Chen, J., Pan, L., Zhao, R., Li, Y., 2022. A soybean sodium/hydrogen exchanger GmNHX6 confers plant alkaline salt tolerance by regulating Na+/K+ homeostasis. Front. Plant Sci. *13*, 938635. https://doi.org/10.3389/fpls.2022.938635.

Jing, Y., Shi, L., Li, X., Zheng, H., Gao, J., Wang, M., Zhang, W., 2019. OXS2 is required for salt tolerance mainly through associating with salt Inducible genes, CA1 and Araport11, in Arabidopsis. Sci. Rep. *9* (1), 1–11. https://doi.org/10.1038/s41598-019-56456-1.

Kalaji, H.M., Rastogi, A., Živčák, M., Brestic, M., Daszkowska-Golec, A., Sitko, K., Alsharafa, K.Y., Lotfi, R., Stypiński, P., Samborska, I.A., Cetner, M.D., 2018. Prompt chlorophyll fluorescence as a tool for crop phenotyping: an example of barley landraces exposed to various abiotic stress factors. Photosynthetica 56 (3), 953–961. https://doi.org/10.1007/s11099-018-0766-z.

Kazan, K., Manners, J.M., 2012. JAZ repressors and the orchestration of phytohormone crosstalk. Trends Plant Sci. *17* (1), 22–31. https://doi.org/10.1016/j.tplants.2011.10.006.

Kazan, K., Manners, J.M., 2013. MYC2: the master in action. Mol. Plant 6 (3), 686–703.

Kotake, T., Dina, S., Konishi, T., Kaneko, S., Igarashi, K., Samejima, M., Tsumuraya, Y., 2005. Molecular cloning of a β-galactosidase from radish that specifically hydrolyzes β-(1→ 3)-and β-(1→ 6)-galactosyl residues of arabinogalactan protein. Plant Physiol. *138* (3), 1563–1576. https://doi.org/10.1104/pp.105.062562.

Kroh, G.E., Pilon, M., 2020. Regulation of iron homeostasis and use in chloroplasts. Int. J. Mol. Sci. *21* (9), 3395. https://doi.org/10.3390/ijms21093395.

Langmead, B., Salzberg, S.L., 2012. Fast gapped-read alignment with Bowtie 2. Nat. Methods *9* (*4*), 357–359. https://doi.org/10.1038/nmeth.1923.

Li, B., Dewey, C.N., 2011. RSEM: accurate transcript quantification from RNA-Seq data with or without a reference genome. BMC Bioinforma. *12* (1), 1–16. https://doi.org/10.1093/ASp/ASm009.

Li, J., Guo, Y., Yang, Y., 2022. The molecular mechanism of plasma membrane H+-ATPases in plant responses to abiotic stress. J. Genet. Genom. https://doi.org/10.1016/j.jgg.2022.05.007.

Li, N., Liu, H., Sun, J., Zheng, H., Wang, J., Yang, L., Zou, D., 2018. Transcriptome analysis of two contrasting rice cultivars during alkaline stress. Sci. Rep. *8* (*1*), 1–16. https://doi.org/10.1038/s41598-018-27940-x.

Liu, L., Chen, M., Xu, X., Su, Z., tang, J., Gong, J., Zhang, X., Yi, Y., 2024. Bicarbonate affects the expression of iron acquisition genes involved in chlorosis in *Medicago lupulina*. Acta Physiol. Plant. 46, 46–55. https://doi.org/10.1007/s11738-024-03685-1.

Liu, L., Wang, B., 2021. Protection of halophytes and their uses for cultivation of saline-alkali soil in China. Biology 10 (5), 353. https://doi.org/10.3390/biology10050353.

Llugany, M., Martin, S.R., Barceló, J., Poschenrieder, C., 2013. Endogenous jasmonic and salicylic acids levels in the Cd-hyperaccumulator *Noccaea (Thlaspi) praecox* exposed to fungal infection and/or mechanical stress. Plant Cell Rep. 32 (8), 1243–1249. https://doi.org/10.1007/s00299-013-1427-0.

Lopez-Millan, A.F., Grusak, M.A., Abadia, A., Abadía, J., 2013. Iron deficiency in lants: an insight from proteomic approaches. Front. Plant Sci. 4, 254.

Love, M.I., Huber, W., Anders, S., 2014. Moderated estimation of fold change and dispersion for RNA-seq data with DESeq2. Genome Biol. *15*, 550. https://doi.org/10.1186/s13059-014-0550-8.

Lovelli, S., Scopa, A., Perniola, M., Di Tommaso, T., Sofo, A., 2012. Abscisic acid root and leaf concentration in relation to biomass partitioning in salinized tomato plants. J. Plant Physiol. 169 (3), 226–233. https://doi.org/10.1016/j.jplph.2011.09.009.

Lucena, J.J., 2000. Effects of bicarbonate, nitrate and other environmental factors on iron deficiency chlorosis. A review. J. Plant Nutr. 23 (11-12), 1591–1606. https://doi.org/10.1080/01904160009382126.

Marconi, G., Pace, R., Traini, A., Raggi, L., Lutts, S., Chiusano, M., Albertini, E., 2013. Use of MSAP markers to analyse the effects of salt stress on DNA methylation in rapeseed (*Brassica napus* var. oleifera). PloS One *8* (*9*), e75597. https://doi.org/10.1371/journal.pone.0075597.

Markakis, M.N., Boron, A.K., Van Loock, B., Saini, K., Cirera, S., Verbelen, J.P., Vissenberg, K., 2013. Characterization of a small auxin-up RNA (SAUR)-like gene involved in Arabidopsis thaliana development. PloS One *8* (*11*), e82596. https://doi.org/10.1371/journal.pone.0082596.

Maxwell, K., Johnson, G.N., 2000. Chlorophyll fluorescence - a practical guide. J. Exp. Bot. *51* (*345*), 659–668. https://doi.org/10.1093/jexbot/51.345.659.

McClellan, C.A., Chang, C., 2008. The role of protein turnover in ethylene biosynthesis and response. Plant Sci. *175* (*1-2*), 24–31. https://doi.org/10.1016/j.plantsci.2008.01.004.

Meng, C., Quan, T.Y., Li, Z.Y., et al., 2017. Transcriptome profiling reveals the genetic basis of alkalinity tolerance in wheat. BMC Genom. 18, 24. https://doi.org/10.1186/s12864-016-3421-8.

Moeder, W., Ung, H., Mosher, S., Yoshioka, K., 2010. SA-ABA antagonism in defense responses. Plant Signal. Behav. *5* (10), 1231–1233. https://doi.org/10.4161/psb.5.10.12836.

Moneo-Sánchez, M., Izquierdo, L., Martín, I., Labrador, E., Dopico, B., 2016. Subcellular location of *Arabidopsis thaliana* subfamily a1 β-galactosidases and developmental regulation of transcript levels of their coding genes. Plant Physiol. Biochem. *109*, 137–145. https://doi.org/10.1016/j.plaphy.2016.09.016.

Pai, A.A., Pritchard, J.K., Gilad, Y., 2015. The genetic and mechanistic basis for variation in gene regulation. PLoS Genet. *11* (1), e1004857. https://doi.org/10.1016/j.plaphy.2016.09.016.

Pan, X., Welti, R., Wang, X., 2008. Simultaneous quantification of major phytohormones and related compounds in crude plant extracts by liquid chromatography–electrospray tandem mass spectrometry. Phytochemistry 69 (8), 1773–1781.

Peixoto, B., Moraes, T.A., Mengin, V., Margalha, L., Vicente, R., Feil, R., Baena-González, E., 2021. Impact of the SnRK1 protein kinase on sucrose homeostasis and the transcriptome during the diel cycle. Plant Physiol. *187* (3), 1357–1373. https://doi.org/10.1093/plphys/kiab350.

Pérez-Martín, L., Busoms, S., Almira, M.J., Azagury, N., Terés, J., Tolrà, R., Barcelo, J., 2022. Evolution of salt tolerance in *Arabidopsis thaliana* on siliceous soils does not confer tolerance to saline calcareous soils. Plant Soil 1–21. https://doi.org/10.1007/s11104-022-05439-9.

Pérez-Martín, L., Busoms, S., Tolrà, R., Poschenrieder, C., 2021. Transcriptomics reveals fast changes in salicylate and jasmonate signaling pathways in shoots of carbonate-tolerant *Arabidopsis thaliana* under bicarbonate exposure. Int. J. Mol. Sci. 22 (3), 1226. https://doi.org/10.3390/ijms22031226.

Pérez-Martín, L. (2021). Physiological, molecular and genetic mechanisms of adaptation to alkaline and saline soils in Arabidopsis thaliana populations.

Price, L., Han, Y., Angessa, T., Li, C., 2022. Molecular Pathways of WRKY Genes in Regulating Plant Salinity Tolerance. Int. J. Mol. Sci. *23* (18), 10947. https://doi.org/10.3390/ijms231810947.

Putri, G.H., Anders, S., Pyl, P.T., Pimanda, J.E., Zanini, F., 2022. Analysing high-throughput sequencing data in Python with HTSeq 2.0. Bioinformatics *38* (*10*), 2943–2945. https://doi.org/10.1093/bioinformatiNS/btac166.

Rai, S., Singh, P.K., Mankotia, S., Swain, J., Satbhai, S.B., 2021. Iron homeostasis in plants and its crosstalk with copper, zinc, ad manganese. Plant Stress 1, 100008. https://doi.org/10.1016/j.stress.2021.100008.

Rasmussen, S., Barah, P., Suarez-Rodriguez, M.C., Bressendorff, S., Friis, P., Costantino, P., Mundy, J., 2013. Transcriptome responses to combinations of stresses in Arabidopsis. Plant Physiol. *161* (4), 1783–1794. https://doi.org/10.1104/pp.112.210773.

Riemann, M., Dhakarey, R., Hazman, M., Miro, B., Kohli, A., Nick, P., 2015. Exploring jasmonates in the hormonal network of drought and salinity responses. Front. Plant Sci. *6*, 1077. https://doi.org/10.3389/fpls.2015.01077.

Römheld, V., 1987. Different strategies for iron acquisition in higher plants. Physiol. Plant. 70 (2), 231–234. https://doi.org/10.1111/j.1399-3054.1987.tb06137.x.

Römheld, V., 2000. The chlorosis paradox: Fe inactivation as a secondary event in chlorotic leaves of grapevine. J. Plant Nutr. 23 (11-12), 1629–1643. https://doi.org/10.1080/01904160009382129.

Ross, G.S., Wegrzyn, T., MacRae, E.A., Redgwell, R.J., 1994. Apple [beta]-Galactosidase (Activity against Cell Wall Polysaccharides and Characterization of a Related cDNA Clone). Plant Physiol. *106* (2), 521–528. https://doi.org/10.1104/pp.106.2.521.

Rus, A., Baxter, I., Muthukumar, B., Gustin, J., Lahner, B., Yakubova, E., Salt, D.E., 2006. Natural variants of At HKT1 enhance Na+ accumulation in two wild populations of Arabidopsis. PLoS Genet. *2* (12), e210. https://doi.org/10.1371/journal.pgen.0020210.

Sah, S.K., Reddy, K.R., Li, J., 2016. Abscisic acid and abiotic stress tolerance in crop plants. Front. Plant Sci. *7*, 571. https://doi.org/10.3389/fpls.2016.00571.

Sazegari, S., Niazi, A., Ahmadi, F.S., 2015. A study on the regulatory network with promoter analysis for Arabidopsis DREB-genes. Bioinformation 11 (2), 101. https://doi.org/10.6026/97320630011101.

Segarra, G., Jáuregui, O., Casanova, E., Trillas, I., 2006. Simultaneous quantitative LC–ESI-MS/MS analyses of salicylic acid and jasmonic acid in crude extracts of Cucumis sativus under biotic stress. Phytochemistry *67* (*4*), 395–401. https://doi.org/10.1016/j.phytochem.2005.11.017.

Shabala, S., Cuin, T.A., 2008. Potassium transport and plant salt tolerance. Physiol. Plant. *133* (*4*), 651–669. https://doi.org/10.1111/j.1399-3054.2007.01008.x.

Singh, A., 2021. Soil salinization management for sustainable development: A review. J. Environ. Manag. *277*, 111383. https://doi.org/10.1016/j.jenvman.2020.111383.

Skalak, J., Nicolas, K.L., Vankova, R., Hejatko, J., 2021. Signal integration in plant abiotic stress responses via multistep phosphorelay signaling. Front. Plant Sci. *12*, 644823. https://doi.org/10.3389/fpls.2021.644823.

Smith, D.L., Gross, K.C., 2000. A family of at least seven β-galactosidase genes is expressed during tomato fruit development. Plant Physiol. *123* (3), 1173–1184. https://doi.org/10.1104/pp.123.3.1173.

Spartz, A.K., Ren, H., Park, M.Y., Grandt, K.N., Lee, S.H., Murphy, A.S., Gray, W.M., 2014. SAUR inhibition of PP2C-D phosphatases activates plasma membrane $H^+$-ATPases to promote cell expansion in Arabidopsis. Plant Cell *26* (*5*), 2129–2142. https://doi.org/10.1105/tAS.114.126037.

Sun, Y., Hao, P., Lv, X., Tian, J., Wang, Y., Zhang, X., Wu, T., 2020. A long non-coding apple RNA, MSTRG. 85814.11, acts as a transcriptional enhancer of SAUR32 and contributes to the Fe-deficiency response. Plant J. *103* (1), 53–67. https://doi.org/10.1111/tpj.14706.

Terés, J., Busoms, S., Perez Martín, L., Luís-Villarroya, A., Flis, P., Álvarez-Fernández, A., Poschenrieder, C., 2019. Soil carbonate drives local adaptation in *Arabidopsis thaliana*. Plant, Cell Environ. *42* (*8*), 2384–2398. https://doi.org/10.1111/ASe.13567.

Wang, N., Fan, X., Lin, Y., Li, Z., Wang, Y., Zhou, Y., Ma, J., 2022. Alkaline stress induces different physiological, hormonal and gene expression responses in diploid and autotetraploid rice. Int. J. Mol. Sci. *23* (*10*), 5561. https://doi.org/10.3390/ijms23105561.

Wang, X.S., Han, J.G., 2007. Effects of NaCl and silicon on ion distribution in the roots, shoots and leaves of two alfalfa cultivars with different salt tolerance. Soil Sci. Plant Nutr. *53* (*3*), 278–285. https://doi.org/10.1111/j.1747-0765.2007.00135.x.

Wittstock, U., Halkier, B.A., 2002. Glucosinolate research in the Arabidopsis era. Trends Plant Sci. *7* (6), 263–270. https://doi.org/10.1016/S1360-1385(02)02273-2.

Xie, Z., Nolan, T.M., Jiang, H., Yin, Y., 2019. AP2/ERF transcription factor regulatory networks in hormone and abiotic stress responses in Arabidopsis. Front. Plant Sci. *10*, 228. https://doi.org/10.3389/fpls.2019.00228.

Yan, F., Zhu, Y., Zhao, Y., Wang, Y., Li, J., Wang, Q., Liu, Y., 2020. De novo transcriptome sequencing and analysis of salt-, alkali-, and drought-responsive genes in *Sophora alopecuroides*. BMC genomiNS 21 (1), 1–15. https://doi.org/10.1186/s12864-020-06823-4.

Yang, H., Wu, Y., Duan, Y., Zhang, C., Huang, Z., Wu, W., Li, W., 2022. Metabolomics combined with physiological and transcriptomic analyses reveal regulatory features associated with blueberry growth in different soilless substrates. Sci. Hortic. *302*, 111145. https://doi.org/10.1016/j.scienta.2022.111145.

Zandalinas, S.I., Sengupta, S., Fritschi, F.B., Azad, R.K., Nechushtai, R., Mittler, R., 2021. The impact of multifactorial stress combination on plant growth and survival. N. Phytol. 230 (3), 1034–1048. https://doi.org/10.1111/nph.17232.

Zhang, B., Chen, X., Lu, X., Shu, N., Wang, X., Yang, X., Ye, W., 2018. Transcriptome analysis of *Gossypium hirsutum* L. reveals different mechanisms among NaCl, NaOH and Na2CO3 stress tolerance. Sci. Rep. 8 (1), 1–14. https://doi.org/10.1038/s41598-018-31668-z.